ORIGINAL ARTICLE

Gut microbiota-derived short-chain fatty acids ameliorate methamphetamine-induced depression- and anxiety-like behaviors in a Sigmar-1 receptor-dependent manner

Kaikai Zhang[a,†], Lijian Chen[a,†], Jianzheng Yang[a,†], Jiali Liu[a], Jiahao Li[a], Yi Liu[a], Xiuwen Li[a], Long Chen[a], Clare Hsu[a], Jiahao Zeng[a], Xiaoli Xie[b,*], Qi Wang[a,*]

[a]Guangzhou Key Laboratory of Forensic Multi-Omics for Precision Identification, School of Forensic Medicine, Southern Medical University, Guangzhou 510515, China
[b]Department of Toxicology, School of Public Health, Southern Medical University (Guangdong Provincial Key Laboratory of Tropical Disease Research), Guangzhou 510515, China

Abstract Methamphetamine (Meth) abuse can cause serious mental disorders, including anxiety and depression. The gut microbiota is a crucial contributor to maintaining host mental health. Here, we aim to investigate if microbiota participate in Meth-induced mental disorders, and the potential mechanisms involved. Here, 15 mg/kg Meth resulted in anxiety- and depression-like behaviors of mice successfully and suppressed the Sigma-1 receptor (SIGMAR1)/BDNF/TRKB pathway in the hippocampus. Meanwhile, Meth impaired gut homeostasis by arousing the Toll-like receptor 4 (TLR4)-related colonic inflammation, disturbing the gut microbiome and reducing the microbiota-derived short-chain fatty acids (SCFAs). Moreover, fecal microbiota from Meth-administrated mice mediated the colonic inflammation and reproduced anxiety- and depression-like behaviors in recipients. Further, SCFAs supplementation optimized Meth-induced microbial dysbiosis, ameliorated colonic inflammation, and repressed anxiety- and depression-like behaviors. Finally, *Sigmar1* knockout (*Sigmar1*$^{-/-}$) repressed the BDNF/TRKB pathway and produced similar behavioral phenotypes with Meth exposure, and eliminated the anti-anxiety and -depression effects of SCFAs. The activation of SIGMAR1 with fluvoxamine attenuated Meth-induced anxiety- and depression-like behaviors. Our findings indicated that gut

microbiota-derived SCFAs could optimize gut homeostasis, and ameliorate Meth-induced mental disorders in a SIGMAR1-dependent manner. This study confirms the crucial role of microbiota in Meth-related mental disorders and provides a potential preemptive therapy.

1. Introduction

Methamphetamine (Meth) is a highly addictive psychostimulant, and its abuse has been a serious public health problem, globally[1]. According to an epidemiological survey, in 2019, there were over 27 million people reported using Meth (0.5% of the global population)[2]. Meth abuse can cause long-term neuropsychiatric impairments[3–5], while anxiety and depression were reported as the most pervasive mental disorders in Meth abusers[6,7].

Anxiety and depression are ubiquitous mental disorders that affect about 10% global population every year[8]. Accumulating evidence indicates the close association of gut microbiota with anxiety and depression disorders[9–11]. Clinically, microbial dysbiosis is prevalent in patients with depression and is recognized as a risk factor for disease[12]. Fecal microbiota transplantation (FMT) from depression patients confirmed its crucial role in the occurrence and development of depression[10]. In addition, the absence of microbiota could reduce the anxiety-like phenotypes[13] and microbial metabolite 4-ethylphenyl sulfate has been confirmed to promote anxiety[14]. Notably, the interactions between gut microbiota and the brain are highly complex and involve multiple pathways, such as host metabolism, immune regulation, and vagal nerve pathway[15–19]. Through decomposing dietary fibers, microbiota can produce short-chain fatty acids, which maintain intestinal immune homeostasis[20,21] and influence brain behaviors[22,23]. Aging-related decrease in SCFAs induced memory impairment and increased depression-like behavior[24]. Meanwhile, SCFAs presented a close association with chronic stress-induced anxiety[25] and could attenuate chronic social failure stress-mediated depression[26]. These indicate that microbiota-derived SCFAs could be the potential modulator of multiple mental disorders.

Our previous studies have confirmed that Meth exposure can disturb gut microbiota, which participated in Meth-related hepatotoxicity[2]. In addition, in Meth-related conditioned place preference, fecal SCFAs were observed reshaped, accompanied by microbial dysbiosis[27]. Further, the absence of gut microbiota deteriorated the conditioned place preference scores[28], implying the participation of microbiota in Meth-induced neurotoxicity. However, the microbial mechanisms underlying Meth-induced anxiety and depression, and the potential therapeutic effects of SCFAs remain largely unknown.

Sigma-1 receptor (SIGMAR1) is an endoplasmic reticulum chaperone protein widely expressed throughout the brain, which has shown protective effects against multiple mental disorders, including anxiety and depression[29–32]. Its agonist fluvoxamine (Flu) has served as a clinical anti-anxiety and -depression drug[33]. In fact, the activation of SIGMAR1 can promote the secretion of mature brain derived neurotrophic factor (BDNF) from pro-BDNF *via* chaperone activity in the endoplasmic reticulum[34], while BDNF and its receptor tyrosine kinase B (TRKB) were the crucial anti-anxiety and -depression factors[35]. The beneficial effects of SIGMAR1 on Meth-induced neural deficits were also observed, including ameliorating Meth-induced dopamine efflux, repressing drug-seeking brain reward function, and improving locomotor sensitization[36]. Nevertheless, the protective effects of SIGMAR1 against Meth-related anxiety and depression disorders, and its interaction with microbiota-derived SCFAs are still obscure.

In this study, we tested the hypothesis that microbial dysbiosis contributes to Meth-related anxiety and depression, while microbiota-derived SCFAs could modulate these mental disorders in SIGMAR1 dependent manner. Through FMT treatment, we confirmed the involvement of microbial dysbiosis in Meth-induced colonic inflammation, and anxiety and depression. By SCFAs supplementation, we verified its optimization on gut homeostasis and its protection against Meth related-anxiety and -depression. Finally, using *Sigmar1*$^{-/-}$ mice and agonist Flu, we found that the effects of these interventions on Meth-induced mental disorders relied on the modulation of the SIGMAR1/BDNF/TRKB pathway.

2. Materials and methods

2.1. Reagents and antibodies

Methamphetamine (Meth, purity over 99%) was provided by the National Institute for the Control of Pharmaceutical and Biological Products (Beijing, China). Antibiotics were purchased from Sangon Biotech (Shanghai, China): vancomycin (CAS#: 1404-93-9), neomycin sulfate (CAS#: 1405-10-3), metronidazole (CAS#: 443-48-1), and ampicillin (CAS#: 69-52-3). SCFAs were purchased from Sigma−Aldrich (St Louis, MO, USA): sodium acetate (CAS#: 127-09-3) and sodium propionate (CAS#: 137-40-6). Flu was purchased from Macklin (Shanghai, China, CAS#: 54739-18-3). The primary and secondary antibodies for Western blot analysis in this study were listed in Supporting Information Table S1.

2.2. Animals and treatment

Male wild-type (WT) C57BL/6 mice and *Sigmar1*$^{-/-}$ mice on a C57BL/6 background were obtained from Cyagen Biotechnology Co., Ltd. (Guangzhou, China). Mice were bred and housed in a specific pathogen-free-level laboratory animal condition. All animal care and experimental protocols were approved by the Medical Ethics Committee of Southern Medical University (Approval Code: L2020092).

2.2.1. Meth administration
8−10 weeks old WT or *Sigmar1*$^{-/-}$ mice were randomly assigned to the Saline and Meth groups. To induce Meth-related anxiety and depression disorders, mice were intraperitoneally (i.p.)

injected with Meth (15 mg/kg) or equal volume saline at 12 h intervals for 4 consecutive days[37,38]. This dosing regimen was chosen based on the median value of blood Meth concentration in abusers (about 1.3 μmol/L), which was in line with the average concentration in mice at 1 h after the last injections[39,40]. Fecal collections were performed 12 h after the last injections.

2.2.2. Fecal microbiota transplantation treatment (FMT)
FMT was carried out according to the previous study[41]. (1) Preparation of fecal bacterial fluid: feces from donor mice were resuspended in germ-free PBS at 0.1 g/mL and subsequently, centrifuged to isolate the supernatants ($900 \times g$, 3 min); (2) antibiotic pretreatment: an antibiotic cocktail (vancomycin, 100 mg/kg; neomycin sulfate, 200 mg/kg; metronidazole, 200 mg/kg; and ampicillin, 200 mg/kg) was orally administered to recipient WT or $Sigmar1^{-/-}$ mice (6−8 weeks old) once daily for 7 days. Feces were collected to verify the elimination of gut microbiota; (3) FMT: antibiotic pretreated recipients were dosed with fecal bacterial fluid (10 mL/kg) *via* oral gavage once daily for 7 days.

2.2.3. Short-chain fatty acids (SCFAs) supplementation
To investigate the beneficial effects of SCFAs, WT or $Sigmar1^{-/-}$ mice (4−6 weeks age) were pretreated with SCFAs drinking water containing 67.5 mmol/L sodium acetate (AA) and 25 mmol/L sodium propionate (PA) for 3 weeks, while the control mice were provided with the normal drinking water[42,43]. Drinking solutions were refreshed 3 times per week. Then, since Day 22, mice received 4 days' Meth or saline challenges, and the regimen was administrated as previously described. Fecal collection and behavioral tests were carried out at the end of the experimental period (Day 30).

To further identify which SCFA played a major role in protective effects, WT mice were randomly assigned into the Saline group, Meth group, AA + Meth group, PA + Meth group, and SCFAs + Meth group. Mice in the Saline or Meth group were pretreated with normal drinking water for 3 weeks and subsequently, received 15 mg/kg Meth or equal volume Saline challenges for 4 days as described above. Meanwhile, mice in the AA + Meth group, PA + Meth group, and SCFAs + Meth group were respectively pretreated with AA drinking water (containing 67.5 mmol/L sodium acetate), PA drinking water (containing 25 mmol/L sodium propionate), and their mixture SCFAs drinking water (containing 67.5 mmol/L sodium acetate and 25 mmol/L sodium propionate) for 3 weeks[42,43] and then, Meth was i.p. administrated to mice for 4 consecutive days as described above.

2.2.4. Fluvoxamine (Flu) treatment
WT mice (8−10 weeks old) were i.p. administrated with 30 mg/kg Flu or equal volume Saline (once daily) for 7 continuous days[44]. Since Day 4, Meth administration procedures were performed on mice as previously described. Twelve hours after the last injections, fecal samples were collected and then stored at −80 °C for further analysis.

In addition, to investigate the potential microbial mechanisms for the protection of Flu, Meth-administrated mice were orally pretreated with gut microbiota from Flu-treated mice. In detail, fecal samples were mixed thoroughly with germ-free PBS at a ratio of 0.1 g/mL, and the obtained suspension was centrifuged to separate the supernatant for FMT treatment. Similarly, mice were orally administrated with fecal bacterial fluid (10 mL/kg, FMT-Flu) or equal volume germ-free PBS for continuous 7 days[45].

Since Day 4, mice received the Saline or Meth challenges as previously described.

2.3. Behavioral assessments

2.3.1. Open-field test (OFT)
The open field consisted of a grey floor with grey walls (45 cm × 45 cm × 45 cm). Mice were individually placed in the center of the chamber for 6 min of free exploration. A smart video tracking system (version 3.0; PanLab Technology for Bioresearch, Barcelona, Spain) measured the total distance, as well as the time spent in the central zone (10 cm from the walls) during the last 5 min. The fecal number was also recorded.

2.3.2. Elevated plus-maze test (EPMT)
The elevated plus-maze apparatus consisted of a grey crossed maze (two open arms: 30 cm length × 6 cm wide; two closed arms: 30 cm length × 6 cm wide × 15 cm height), and elevated above the ground by approximately 60 cm. Mice were individually placed in the center of the maze to explore freely for 6 min. Similarly, the track during the last 5 min was recorded by the Smart video tracking system.

2.3.3. Tail suspension test (TST)
Mice were individually suspended by their tails using adhesive tape (1−1.5 cm from the tip of the tail) and the head of the mice was 20 cm above the floor. The test sessions lasted for 6 min and only the last 4 min were scored for immobility. A pose without body movement and hanging passively was accepted as immobility.

2.3.4. Forced swim test (FST)
Mice were placed individually in a plastic cylinder (30 cm height × 15 cm diameter) filled with 18 cm water (23−25 °C) for 6 min, and the last 4 min were scored for immobility. The absence of all motion was defined as immobility (except the required movements to keep the head above the water).

2.4. Sample collections

Fecal samples were collected using a metabolic cage 12 h after the last injection or gavage, and they were immediately stored at −80 °C for further analysis. Blood was collected *via* cardiac puncture under pentobarbital anesthesia (50 mg/kg) after the behavioral tests were completed. The mice were then transcardially perfused with either saline or 4% cold paraformaldehyde. Colonic and hippocampal tissues from mice perfused with saline were immediately dissociated and stored at −80 °C, while colonic tissues and the whole brain from mice perfused with paraformaldehyde were harvested for post-fixation. Blood samples were left at room temperature for 30 min and then centrifuged at $4000 \times g$ for 10 min at 4 °C to separate the serum. The resulting serum samples were stored at −80 °C for further analysis.

2.5. FITC dextran 4-KD (FD4) intestinal permeability experiment

After 6 h fasting and water deprivation, mice were orally administrated with FD4 (average mol wt: 3000−5000, Sigma−Aldrich) at a dose of 600 mg/kg. Four hours later, serum samples were harvested and then, the concentration of FD4 was

measured using a microplate reader (Synergy H1, BioTek) with an excitation wavelength of 485 nm and an emission wavelength of 530 nm.

2.6.   Measurement of lipopolysaccharide (LPS) concentration in serum

To detect the LPS concentration in serum, an enzyme-linked immunosorbent assay (ELISA) kit (Cat#: MM-0634M2, MEIMIAN) was utilized according to the manufacturer's instructions (Jiangsu Meimian Industrial Co., Ltd., Yancheng, China). The OD values were measured using a microplate reader (Synergy H1, BioTek) and the serum LPS concentration was calculated according to the standard curve generated by standard solutions.

2.7.   Histopathology

In brief, 4% paraformaldehyde was used to fix colonic samples for two days. After embedded in paraffin, samples were cut into 5 μm sections for Hematoxylin and Eosin (H&E) staining, periodic acid-Schiff (PAS, Sigma−Aldrich) and Alcian Blue (AB, Sigma−Aldrich) staining, respectively. Slides were observed using a light microscope (Leica DM500, Wetzlal, Germany). The number of goblet cells in each crypt was counted in a blind manner.

2.8.   Immunofluorescence analysis (IF)

Mice were anesthetized and transcardially perfused with 4% cold paraformaldehyde. After harvesting their brain, they were post-fixed in paraformaldehyde at 4 °C overnight. Then, the tissues were embedded into 30% sucrose for cryoprotection for 24 h. For Immunostaining, the brains were coronally cut into 40−60 μm sections using a sliding microtome. Then, 3% hydrogen peroxide was used to inactivate the endogenous peroxide, and the sections were blocked with 3% bovine serum albumin (Sigma−Aldrich). Subsequently, the sections were incubated with the primary antibodies at 4 °C overnight: rabbit-Sigma-1 receptor antibody (1:100, ThermoFisher, Cat#: 42−3300), rabbit-BDNF antibody (1:1000, Abcam, Cat#: ab108319) and rabbit-phospho-TRKB antibody (p-TRKB, 1:200, Bioss, Cat#: bs-5526R). Finally, the sections were incubated with the donkey anti-rabbit IgG H&L secondary antibody (1:500, Life technologies, Cat#: A21207) for 1 h at room temperature. The nucleus was stained with DAPI (Sigma−Aldrich)[46]. Fluorescence was captured using a fluorescence microscope (Leica M165FC, Leica Microsystems, Nussloch, Germany), and the number of positive cells per visual field was counted in a blind manner.

2.9.   Real-time quantitative PCR (RT-qPCR)

Total RNA was extracted from colonic and hippocampal tissue using TRIzol RNA purification reagent (Biomiga, USA). The quality and the quantity of RNA were measured using an ultraviolet−visible spectrophotometer (NanoDrop, 2100 Bioanalyser). Then, the total RNA was reverse-transcribed into complementary DNA (cDNA) using a HiScript II 1st Strand cDNA Synthesis Kit (Vazyme, Nanjing, China). A 7500 real-time PCR system (Applied Biosystems, NY, USA) performed the amplification program using HieffTM qPCR SYBRR Green Master Mix (Low Rox Plus) (YEASEN, Shanghai, China). The expression of target genes was normalized to β-actin

using the $2^{-\Delta\Delta Ct}$ method[47−49]. The primers were listed in Supporting Information Table S2.

2.10.   Western blot analysis

Tissues were lysed using RIPA lysis buffer (Beyotime Biotechnology, Jiangsu, China) with 1% PMSF and 1% phosphatase inhibitor. A BCA protein assay kit was utilized to detect the concentration of protein (ThermoFisher Scientific, USA). Then, equal amounts of total protein (20 μg each sample) were separated by 8%−12% SDS polyacrylamide gel (PAGE) and transferred into a PVDF membrane (Millipore, Billerica, MA, USA). After blocked with 5% skim milk (room temperature, 2 h), membranes were incubated with the primary antibodies (4 °C, overnight) followed by incubation with the appropriate HRP-labelled secondary antibodies (room temperature, 2 h)[50,51]. The target protein bands were visualized using Tanon Gel Image System (version 4.2) and the quantification of bands was performed using Image J software (version 1.8.0). The primary and secondary antibodies are listed in Table S1.

2.11.   RNA sequencing

To reveal the characteristics of colonic transcription level after Meth administration, RNA sequencing was performed by the Majorbio Bio-Pharm Technology Co., Ltd. (Shanghai, China). Briefly, the total RNA was extracted from colonic samples using the TRIzol Reagent (Invitrogen, CA, USA) in accordance with the manufacturer's instructions. The quality and quantity of RNA samples were determined using the NanoDrop2000 (ThermoFisher Scientific, MA, USA) to meet the requirement for Library preparation: the total quantity ≥ 1 μg, concentration ≥ 50 ng/μL, $OD_{260/280} = 1.8−2.2$, RIN ≥ 6.5. The sequencing library was constructed using the Truseq RNA sample prep Kit (Illumina, CA, USA). Next, sequencing was performed by the Majorbio Bio-Pharm Technology Co., Ltd. (Shanghai, China) using the Illumina NovaSeq6000 (Illumina, CA, USA). Sequencing reads were mapped to the reference genome using the TopHat software (version 2.11, https://ccb.jhu.edu/software/tophat/index.shtml) and then counted using HTSeq (version 0.7.1, http://www-huber.embl.de/HTSeq/). Differential expression genes (DEGs) analysis was performed using the DESeq2 (http://bioconductor.org/packages/stats/bioc/DESeq2/) with the screening parameters: fold-change ≥ 1.5 or ≤ 0.67, P-adjust < 0.05. Finally, Gene ontology (GO) functional annotations (http://www.geneontology.org/), Kyoto Encyclopedia of Genes and Genomes (KEGG) analysis (http://www.genome.jp/kegg/), and protein−protein interaction (PPI) analysis (Cytoscape_v3.6.1, http://string-db.org/cgi/input.pl/) were performed on the DEGs for function analysis[38,52].

2.12.   16S rRNA gene sequencing

As described in our previous studies[2,52], microbial DNA was extracted from fecal samples using the E.Z.N.A. soil DNA Kit (Omega Bio-tek, Norcross, GA, US). PCR amplification was performed using an ABI GeneAmp 9700 PCR thermocy'-ACTCCTACGGGAGGCAGCAG-3′ and 806R, 5′-GGACTACHVGGGTWTCTAAT-3′. Subsequently, purified amplicons were sequenced on an Illumina MiSeq platform (Illumina, San Diego, CA, USA) by the Majorbio Bio-Pharm Technology Co., Ltd. (Shanghai, China). Then, the raw 16S rRNA reads were demultiplexed, quality-filtered, and merged based on the Trimmomatic and FLASH

(version 1.2.11). Ultimately, Operational taxonomic units (OTUs) with a 97% similarity cutoff were clustered using UPARSE (version 7.1, http://drive5.com/uparse/). The taxonomy of each OTU representative sequence was analyzed by RDP Classifier version 2.2 against the 16S rRNA database (Silva v138). The rarefaction curve, rank—abundance curve, and community barplot analysis were performed using the R language package (version 3.3.1). The Sankey diagram analysis was carried out on the OmicStudio Cloud Platform (https://www.omicstudio.cn).

2.13. Targeted metabolomics

2.13.1. Fecal samples
SCFAs were extracted from fecal samples (100 mg, each sample) using a methanol mixture containing 10% 2-ethylbutyric acid (1 mg/mL). Next, Gas chromatography—mass spectrometry (GC—MS) analysis was performed on samples using an Agilent 8890B gas chromatography (Agilent, USA) coupled to an Agilent 5977B mass selective detector (Agilent, USA) with an inert electron impact ionization source (Agilent, USA), according to the standard protocols by the Majorbio Bio-Pharm Technology Co., Ltd. (Shanghai, China). Data acquisition was conducted in full scan mode and compounds were identified and quantified using the software of Masshunter (v10.0.707.0, Agilent).

2.13.2. Serum samples
50 μL of serum sample was thoroughly mixed with 100 μL of acetonitrile, and then centrifuged to isolate the supernatant. Subsequently, 20 μL of the supernatant was combined with equal volumes of 3NPH·HCl (200 mmol/L) and EDC·HCl (120 mmol/L, containing 6% pyridine), and the mixture was allowed to react for 30 min. The reaction products were then diluted to 750 μL with a 50% acetonitrile aqueous solution for further analysis. Ultra-high-performance liquid chromatography—mass spectrometry (UHPLC—MS/MS) analysis was conducted on the samples using an ExionLC AD system (Sciex, USA), coupled with a QTRAP 6500+mass spectrometer (Sciex, USA), at Majorbio Bio-Pharm Technology Co., Ltd. (Shanghai, China). The raw data were processed using Sciex software OS for ion fragment identification and integration. Metabolite concentrations within the sample were calculated based on a linear regression standard curve.

2.14. Statistical analysis

Data analyses were performed using the GraphPad Prism software (version 6.0). For serum FD4 and LPS concentration analysis, body weight analysis, behavioral analysis, RT-qPCR analysis, Western blot analysis, and positive cell counting analysis, Student's t-test was employed for two-group comparisons, while multiple-group comparisons were conducted using the One-way ANOVA with Bonferroni correction. For RNA sequencing analysis, the eigenvalue of the covariance matrix method was utilized for principal component analysis (PCA). For 16S rRNA sequencing analysis, the principal composition of samples was analyzed using the principal coordinate analysis (PCoA). Hierarchical clustering was performed using the Unweighted Pair-group Method with Arithmetic Mean (UPGMA). Differential microbiota between two groups were screened using the Wilcoxon rank-sum test, while multiple-group comparisons were performed using the Kruskal—Wallis test. LEfSe cladogram was analyzed using the non-parametric factorial Kruskal—Wallis sum-rank test. Linear discriminant analysis (LDA) was performed to evaluate the contribution degree of differential microbiota for distinguishing among the groups. Correlation analysis was performed by the Spearman correlation analysis. All results are presented as the mean ± standard error of mean (SEM), with the corresponding statistical difference: $^*P < 0.05$, $^{**}P < 0.01$, no sig: no significant difference ($P > 0.05$). All experiments were performed in triplicate at a minimum.
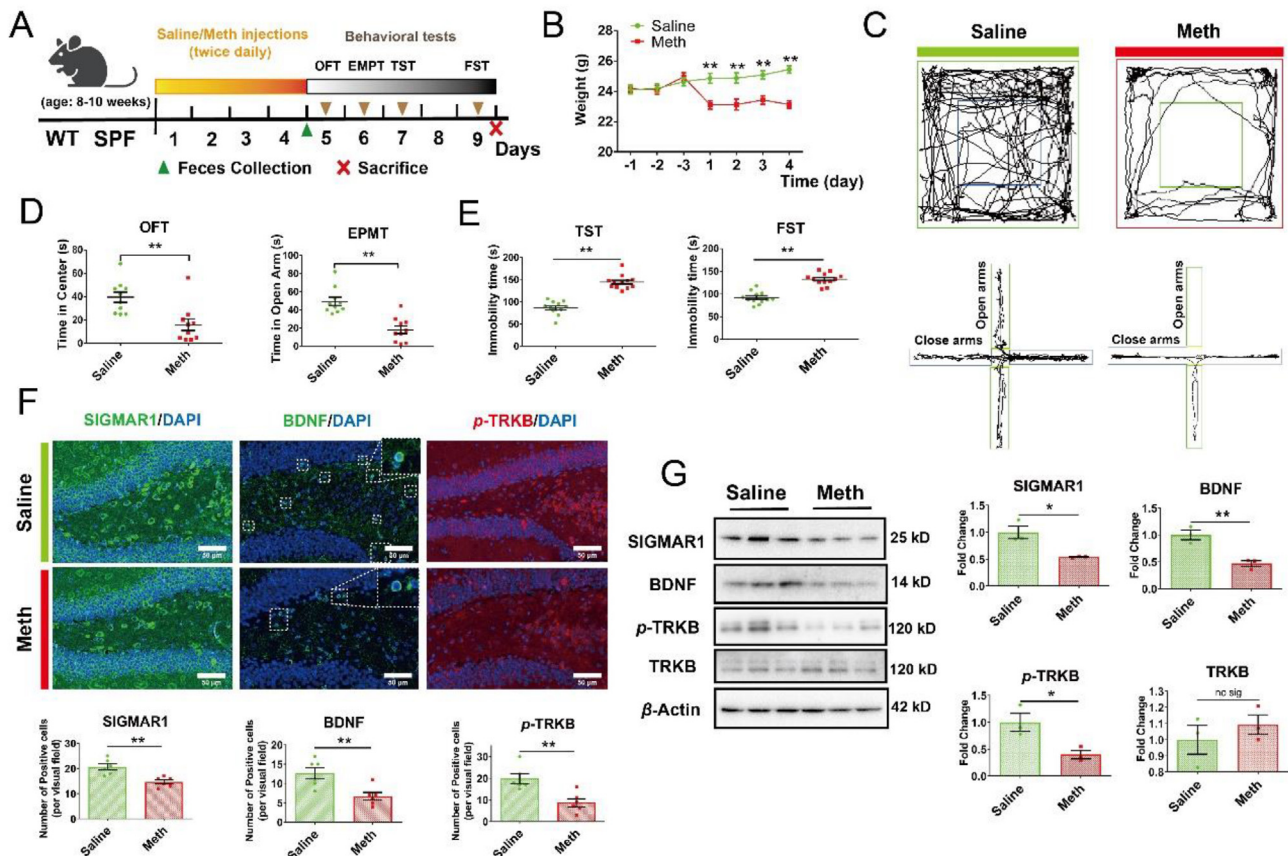
3. Results

3.1. Meth induced anxiety- and depression-like behaviors in mice and repressed the SIGMAR1/BDNF/TRKB pathway of the hippocampus

Meth exposure can cause anxiety and depression in abusers. Here, mice were administrated 15 mg/kg Meth to induce anxiety- and depression-like behaviors (Fig. 1A). We observed that compared to the Saline group, Meth significantly lowered the body weight of mice (Fig. 1B). In the OFT, Meth administration had a significant inhibitory effect on the total travel distance and the time spent in the center zone and displayed an increase in fecal number in comparison with the Saline mice (Fig. 1C and D; Supporting Information Fig. S1A). Meanwhile, the EPMT results showed that the time mice spent in and the number of entries into the open arms was reduced after Meth administration (Fig. 1C and D; Fig. S1B). In addition, Meth significantly elevated immobility time during the TST and FST relative to the Saline group (Fig. 1E). These results indicated that this dosing regimen successfully resulted in anxiety- and depression-like behaviors in mice.

Given the protective effects of SIGMAR1 on anxiety and depression, we determined the expression of the SIGMAR1/BDNF/TRKB pathway in the dentate gyrus (DG) region of the hippocampus, which crucially contributed to anxiety and depression regulation[53]. IF analysis showed that Meth reduced the number of positive cells SIGMAR1, BDNF, and p-TRKB (Fig. 1F). Western blot analysis confirmed these alterations: the expression of proteins SIGMAR1, BDNF, and p-TRKB was reduced after Meth administration in comparison with the Saline mice, and the level of the total TRKB was not altered (Fig. 1G). At the mRNA level, Meth also lowered the level of Sigmar1 and Bdnf, while it had no influence on the expression of mRNA Trkb (Fig. S1C), which was consistent with the protein expression of the total TRKB. Thus, Meth exposure could inhibit the SIGMAR1/BDNF/TRKB pathway in the hippocampus. In addition, we also determined the expression of SIGMAR1 in some other brain regions, including the prefrontal cortex, striatum, and midbrain. Both IF and Western blot analyses revealed no significant difference in SIGMAR1 protein expression in the prefrontal cortex and striatum after Meth exposure compared to the saline group. However, a decrease was observed in the midbrain (Fig. S1D—S1I), suggesting region-specific effects of Meth on SIGMAR1 expression in the brain.

3.2. Meth impaired the gut homeostasis by arousing colonic inflammation, disturbing gut microbiota, and reshaping the composition of SCFAs

The microbiota—gut—brain axis has emerged a crucial role in the regulation of multiple mental disorders, including anxiety and

Figure 1 Meth induced anxiety- and depression-like behaviors of mice, and inhibited the SIGMAR1/BDNF/TRKB pathway in the hippo-campus. (A) Schematic diagram of the experimental procedure. (B) Body weight change curves from three days prior to dose initiation till the end of final dose administration ($n = 9-10$ per group). (C) The representative trajectory diagrams in the OFT and EPMT. (D) The time mice spent in the center zone during the OFT and the time mice spent in the open arms during the EPMT ($n = 10$ per group). (E) The total immobility time during the TST and FST ($n = 11-12$ per group). (F) IF staining of SIGMAR1 (in green), BDNF (in green), and p-TRKB (in red). Nuclei were labeled with DAPI (in blue). The number of positive cells was shown ($n = 6$ per group). Scale bar, 50 μm. (G) Expression of proteins SIGMAR1, BDNF, p-TRKB, the total TRKB, and β-actin was analyzed by Western blot. β-Actin served as a loading control. $n = 3$ per group. Data are expressed as mean ± SEM, $*P < 0.05$, $**P < 0.01$, no sig: no significant difference ($P > 0.05$). All experiments were performed in triplicate at a minimum.

depression[9−11]. Thus, we determined the impacts of Meth on gut homeostasis.

3.2.1. Meth damaged the intestinal barrier function and aroused TLR4-related colonic inflammation

As shown in Fig. 2A, Meth significantly reduced the length of the colon relative to the Saline group. HE staining displayed that Meth caused the larger volume and the "balloon-like" changes of goblet cells (Fig. 2B). Further, AB and PAS staining presented an increased number of AB$^+$ and PAS$^+$ goblet cells after Meth administration (Fig. 2B), indicating that Meth promoted the hyperplasia of goblet cells and increased mucus secretion. Meanwhile, we observed damaged intestinal barrier function after the Meth group, as demonstrated by increased intestinal permeability to FITC-dextran and serum LPS level (Fig. 2C).

To further reveal the molecular mechanisms of Meth-induced colonic impairment, mRNA sequencing was performed. According to the principal component analysis, Meth exposure led to the alteration of colonic components relative to the Saline group (Fig. 2D). Through the screening of DEGs, Meth resulted in a total of 1246 DEGs in the colon relative to the Saline group, containing

693 up-regulated and 553 down-regulated DEGs (Fig. 2E). Furthermore, 87 pathways involved in Meth-induced colonic toxicity were enriched based on KEGG analysis (Supporting Information Table S3). The immune system was identified both in KEGG and GO annotation analysis (Fig. 2F and G; Supporting Information Fig. S2), while the inflammation-related Toll-like receptor signaling pathway and NOD-like receptor signaling pathway were also enriched (Fig. 2H), implying the occurrence of colonic inflammation. Interestingly, Amphetamine addiction was significantly enriched, implying the involvement of the gut−brain axis in Meth addiction (Fig. 2G). Additionally, *Tlr4* was identified as the core gene by the PPI analysis (Fig. 2I), which was the classical target of microbiota-derived LPS[54]. Correspondingly, the expression of protein TLR4 and its downstream nuclear phospho-nuclear factor-κB (p-NF-κB) was upregulated by Meth, while the total NF-κB remained unchanged (Fig. 2J). Meanwhile, Meth elevated the expression of inflammatory factors at the mRNA level, including tumor necrosis factor-α (*Tnf-α*), interleukin-6 (*Il-6*), and interleukin-1β (*Il-1β*) (Fig. 2K). Corresponding to increased intestinal permeability, the tight junction proteins zona occludens 1 (ZO-1) and OCCLUDIN were significantly down-regulated after
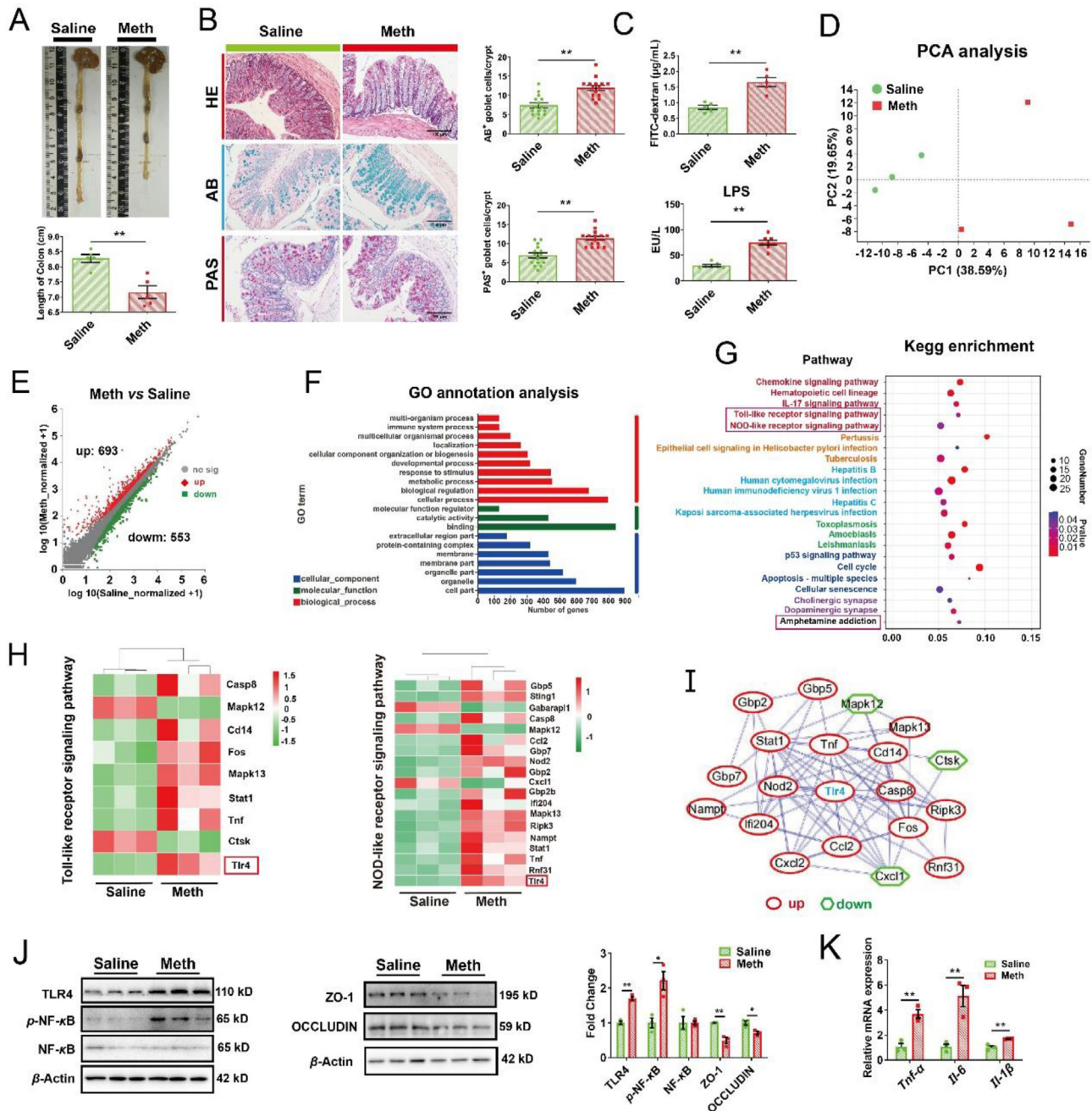
Figure 2 Meth aroused colonic inflammation by activating the TLR4/NF-κB pathway. (A) The representative images and the length of the colon in the Saline and Meth groups were shown ($n = 5$ per group). (B) The representative images of HE, AB, and PAS staining of colonic sections from mice. The number of AB^{+} and PAS^{+} goblet cells per crypt was shown (three random visual fields for each sample, $n = 15$ per group). Scale bar, 150 μm. (C) The concentration of FITC-dextran and LPS in serum ($n = 5-7$ per group). (D) PCA plot analysis of Saline (green dots) and Meth samples (red squares) ($n = 3$ per group). (E) The Scatter-plot graphs of the differential expression genes between Saline and Meth groups: the red rhombuses represented upregulated genes, the green squares represented downregulated genes and the grey dots represented no significant difference. (F) GO analysis of DEGs in the colon. DEGs were annotated to 10 biological processes (red), 7 cellular components (blue), and 3 molecular functions (green) according to the functional classification. (G) KEGG enrichment analysis of DEGs. Red font represents the pathways belonging to the second category of the Immune system; orange font belongs to the Infectious disease: bacterial; wathet blue font belongs to the Infectious disease: viral; green font belongs to the Infectious disease: parasitic; dark blue font belongs to the Cell growth and death; purple font belongs to the Nervous system; black font belongs to the Substance dependence. (H) Heatmaps of gene expression profiles enriched into the Toll-like receptor signaling pathway and the NOD-like receptor signaling pathway. (I) PPI analysis of DEGs enriched into these two pathways. (J) Expression of proteins TLR4, p-NF-κB, the total NF-κB, ZO-1, OCCLUDIN, and β-actin was analyzed by Western blot. β-Actin served as a loading control ($n = 3$ per group). (K) Relative expression of mRNA *Tnf-α*, *Il-6*, and *Il-1β* was normalized by β-actin mRNA ($n = 3$ per group). Data are expressed as mean ± SEM, *$P < 0.05$, **$P < 0.01$, no sig: no significant difference ($P > 0.05$). All experiments were performed in triplicate at a minimum.

Meth administration (*P*-value < 0.05) (Fig. 2J). These results indicated that Meth could arouse colonic inflammation by activating the TLR4/NF-κB pathway and damage the intestinal barrier function.

3.2.2. Meth disturbed gut microbiota and reshaped the composition of SCFAs

16S rRNA sequencing was performed to profile the gut microbiome. Rank-Abundance curves presented similar OTU abundance or evenness among all samples (Fig. 3A). In Alpha diversity, Meth exposure resulted in a higher richness than the Saline group (up-regulated ACE, Chao, and Sobs indexes), while no changes were observed in microbial diversity and coverage (demonstrated by Shannon, Simpson, and Coverage indexes) (Fig. 3A; Supporting Information Fig. S3A−S3E). In Beta diversity, the principal composition of Meth samples was significantly different from that of the Saline group (Fig. 3B), which was in accord with the Hierarchical clustering analysis (Fig. S3F). At the Phylum level, Meth induced a higher abundance of Firmicutes and Deferribacterota, as well as the lower Bacteroidate and Proteobacteria (Fig. 3C; Fig. S3G). Moreover, the ratio of Firmicutes/Bacteroidate was significantly upregulated by Meth administration (Fig. 3D), indicating a worse intestinal environment[55]. At the Family level, Meth altered the abundance of 17 microbes, including 10 upregulated (major Lactobacillaceae, Rikenellaceae, and Deferribacteraceae) and 7 down-regulated microbes (major Muribaculaceae, Sutterellaceae, and Erysipelotrichaceae) (Fig. S3H−S3I). At the Genus level, the SCFAs producers Lactobacillus, Lachnospiraceae_NK4A136_group, and pathogenic Alistipes and Mucispirillum were increased by Meth administration, whereas probiotics norank_f_Muribaculaceae and Faecalibaculum were decreased (Fig. 3E; Fig. S3J). The differential microbiota from Phylum to Genus level were summarized using the LEfSe cladogram and linear discriminant analysis (Fig. 3F and G). The Sankey diagram further revealed the relative abundance of differential microbiota at Phylum and their taxon relationship with the differential microbiota at the Genus level (Fig. S3K). These results suggested that Meth could disturb the gut microbiome and alter SCFAs-related microbes.

Thus, we determined the composition of SCFAs in feces. Among 8 SCFAs, Meth effectively decreased the level of acetic acid, propanoic acid, valeric acid, isobutyric acid, and isovaleric acid, while there were no significant changes in butanoic acid, hexanoic acid, and isohexanoic acid (Fig. 3H). Spearman correlation analysis was performed to reveal the potential association between gut microbiota (Genus level) and SCFAs concentration, behavioral indexes, colonic indexes, and IF indexes (Fig. 3I). The results showed that the abundance of norank_f_Muribaculaceae, Faecalibaculum, norank_f_Desulfovibrionaceae, Helicobacter, Alloprevotella, Dubosiella, Bifidobacterium, Parasutterella, and Desulfovibrio was positively correlated with body weight, colonic length, fecal SCFAs concentration and the expression of SIGMAR1, BDNF, and p-TRKB, while negatively correlated with the number of AB⁺ and PAS⁺ goblet cells, FD4 level and the depression- and anxiety-like behaviors. Meanwhile, the abundance of Lactobacillus, Alistipes, Lachnospiraceae_NK4A136_group, Mucispirillum, Rikenellaceae_RC9_gut_group, and Roseburia presented a positive correlation with the FD4 level, the number of AB⁺ and PAS⁺ goblet cells, and the depression- and anxiety-like behaviors, while presented a negative correlation with the body weight, colonic length, SCFAs concentration and the expression of SIGMAR1, BDNF, and p-TRKB (Fig. 3I). These results indicated

the potential modulation of gut microbiota on colonic damage and behavioral deficits. Furthermore, the composition of serum SCFAs was also assessed following Meth exposure. As observed in fecal samples, Meth primarily reduced the concentration of serum Acetic acid and propanoic acid (Supporting Information Fig. S4A and S4B), and did not exert a significant effect on butanoic acid (Fig. S4C). Additionally, the level of hexanoic acid in serum decreased with Meth administration, whereas there were no statistically significant differences in the levels of valeric acid, isobutyric acid, isovaleric acid, or isohexanoic acid (Fig. S4D−S4H).

3.3. Microbiota from Meth-administrated mice aroused colonic inflammation and further induced anxiety- and depression-like behavior in the recipient mice

Here, we transplanted the microbiota from Meth- and Saline-administrated mice into recipient mice to explore the underlying microbial mechanisms (Fig. 4A). Previously, we did not detect the concentration of Meth and its main metabolite-amphetamine in fecal samples, while we did detect them in serum samples (Meth: 3.728 ± 0.3496 ng/mL; amphetamine: 0.2737 ± 0.04802 ng/mL, mean ± SEM, *n* = 8)[2]. The results excluded the influences of drug residue in feces.

3.3.1. Microbiota from Meth-administrated mice aroused colonic inflammation and damaged intestinal barrier function

As the sequencing depth increased, the rarefaction curves of Shannon and Sobs indexes in antibiotic-pretreated mice were not elevated in comparison to the PBS-pretreated mice, suggesting the elimination of gut microbiota (Fig. 4B). Next, FMT was performed on the recipients. Compared with FMT-C, we observed that FMT-M lowered the body-weight of recipients from day 4 of FMT and this tendency continued until the end of the procedure (Fig. 4C). Corresponding to Meth-administrated mice, there was no significant difference in OTU abundance or evenness among samples (Fig. 4D). FMT-M also increased the richness of the microbiome by elevating the ACE, Chao, and Sobs indexes in comparison with the FMT-C group (Fig. 4D; Supporting Information Fig. S5A and S5B). And diversity was observed to increase by FMT-M: up-regulated Shannon index and down-regulated Simpson index (Fig. S5C and S5D). In addition, Beta diversity presented that the principal composition of FMT-M samples differed from FMT-C according to the PCoA analysis (Fig. 4E). The microbial composition of FMT-M from Phylum to Genus level was significantly different from FMT-C (Fig. 4F; Fig. S5E−S5G). The Sankey diagram further revealed the relative abundance of differential microbiota at the Phylum level and their taxon relationships with differential microbiota at the Genus level (Fig. 4F). These results indicated that we successfully transplanted the microbial community into the recipients.

Furthermore, FMT-M enlarged the size of goblet cells compared to FMT-C. The number of AB⁺ and PAS⁺ goblet cells was elevated by FMT-M (Fig. 4G), suggesting the promotion of proliferation in goblet cells. Moreover, FMT-M significantly reduced the length of the colon and increased the intestinal permeability, as demonstrated by the higher FITC-dextran and LPS level in serum (Fig. 4H). As observed in Meth-administrated mice, FMT-M also aroused colonic inflammation by up-regulating the expression of proteins TLR4 and nuclear p-NF-κB (the total NF-κB was not changed), as well as increasing the mRNA level of *Tnf-α*, *Il-6*, and *Il-1β* (Fig. 4I and J). Consisting of the
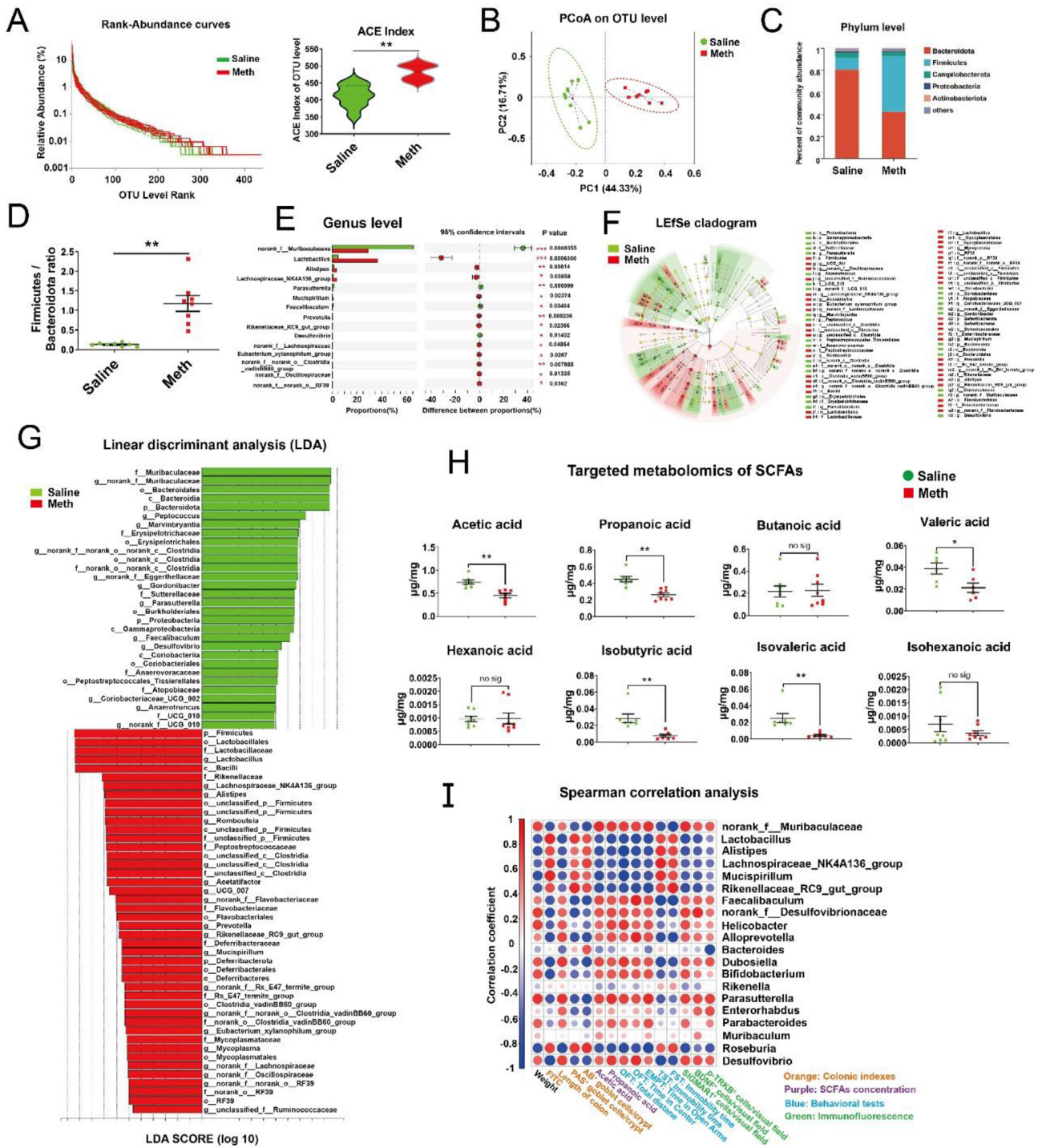
Figure 3 Meth disturbed the gut microbiome and reshaped the composition of fecal SCFAs. (A) The Rank-Abundance Curves of all samples: the abscissa denoted the ranking level of OTU number and the corresponding ordinate denoted the relative percentage; and the alteration of alpha diversity: ACE index at OTU level ($n = 8-9$ per group). (B) PCoA plot analysis. (C) Relative abundance of microbiota at the Phylum level. (D) The ratio of phylum Firmicutes/Bacteroidate. (E) The top 15 differential microbiota between the Saline and Meth groups at the genus level. (F) LEfSe cladogram indicated that multiple taxa are differentially enriched in the corresponding groups. The circles from the inner to the outer circles indicate the phylum, class, order, family, and genus levels. (G) Histogram of linear discriminant analysis (LDA) in the abundance of gut microbiota. Wilcoxon rank-sum test with a 95% confidence interval was performed to screen the differential microbiota. (H) The concentration of SCFAs in the Saline and Meth group, including acetic acid, propanoic acid, butanoic acid, valeric acid, hexanoic acid, isobutyric acid, isohexanoic acid, and isovaleric acid ($n = 6-8$ per group). (I) Spearman correlation analysis of differential microbiota with colonic, behavioral indicators, SCFAs concentration, and IF. The color of the dots denoted the correlation coefficient and the size of the dots represented the P-value. Red dots represent a positive correlation, while the blue ones represent a negativ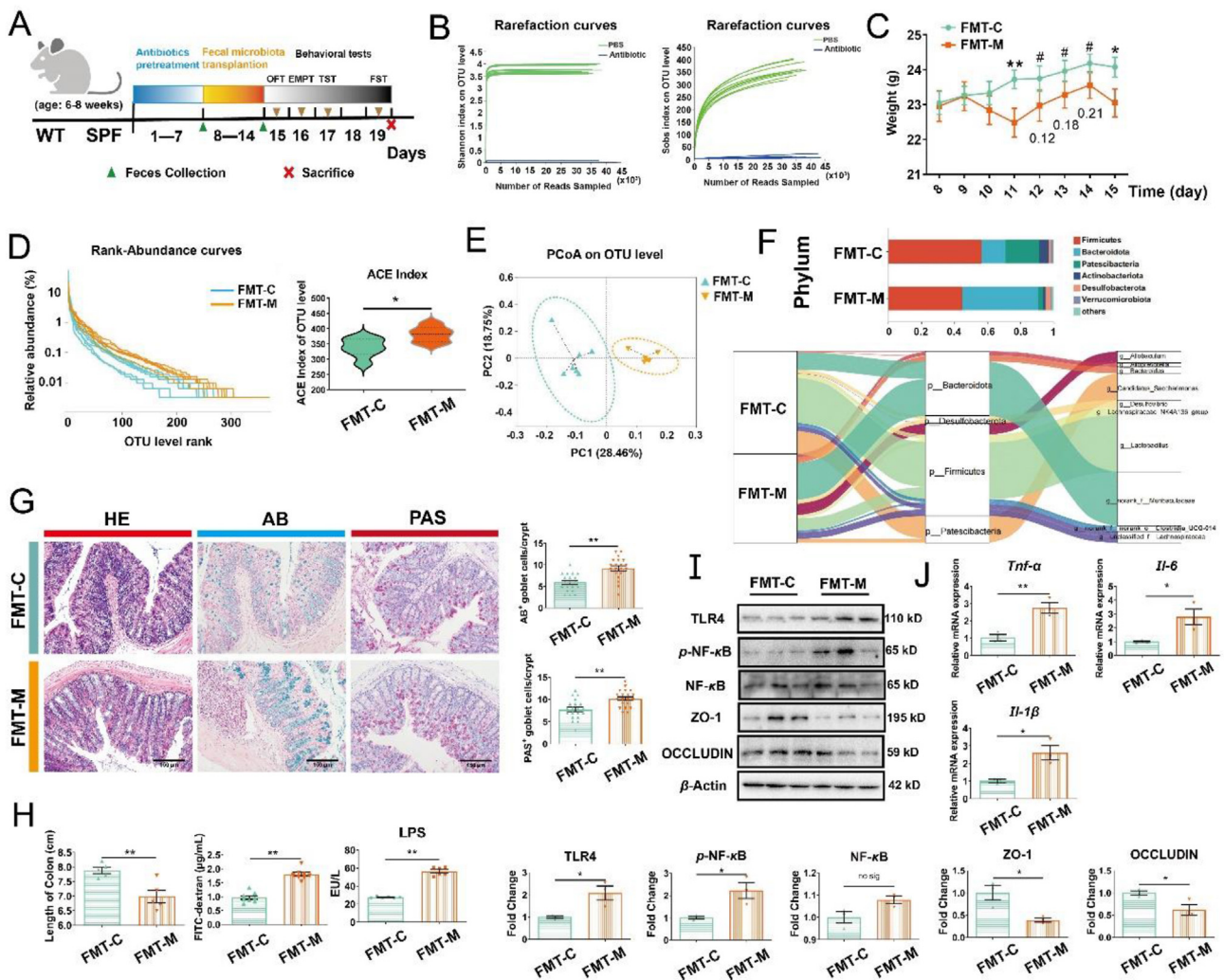e correlation. Data are expressed as mean ± SEM, *$P < 0.05$, **$P < 0.01$, no sig: no significant difference ($P > 0.05$).

Figure 4 Microbiota from Meth-administrated mice induced colonic inflammation by activating the TLR4/NF-κB pathway. (A) Schematic diagram of the experimental procedure. (B) Rarefaction curves of samples in PBS and Antibiotic group ($n = 8$ per group). (C) Body weight change curves ($n = 7-9$ per group). (D)The Rank-Abundance Curves of all samples and the alteration of alpha diversity: ACE index at the OTU level ($n = 6-7$ per group). (E) PCoA plot analysis. (F) Relative abundance of microbiota at the Phylum level and Sankey diagram: relative abundance of differential microbiota at the Phylum level and the corresponding flows of Genus differential microbiota. The color of the ribbon represented the differential microbiota and its width represented the relative abundance of differential microbiota. (G) The representative images of HE, AB, and PAS staining of colonic sections from mice ($n = 6$ per group). Scale bar, 150 μm. The number of AB$^+$ and PAS$^+$ goblet cells per crypt was shown (three random visual fields for each sample) ($n = 20$ per group). (H) The length of the colon ($n = 5$ per group), the concentration of FITC-dextran ($n = 8$ per group), and LPS in the serum ($n = 6$ per group). (I) Expression of proteins TLR4, p-NF-κB, total NF-κB, ZO-1, OCCLUDIN, and β-actin analyzed by Western blot ($n = 3$ per group). (J) Relative expression of mRNA *Tnf-α*, *Il-6* and *Il-1β* ($n = 3$ per group). Data are expressed as mean ± SEM, *$P < 0.05$, **$P < 0.01$, #$P > 0.05$, no sig: no significant difference ($P > 0.05$). All experiments were performed in triplicate at a minimum.

increased intestinal permeability, the expression of ZO-1 and OCCLUDIN was decreased by FMT-M (Fig. 4I). Thus, we certified that gut microbiota participated in Meth-induced colonic inflammation *via* activating TLR4/NF-κB pathway and damaged intestinal barrier.

3.3.2. Microbiota from Meth-administrated mice repressed the SIGMAR1/BDNF/TRKB pathway and induced anxiety- and depression-like behaviors

Given the regulatory effects of microbiota on mental disorders[56], we evaluated the extent of depression and anxiety after FMT-M administration. Behavioral results showed that FMT-M resulted in

shorter total travel distance, lesser time spent in the center zone and more feces in OFT (Fig. 5A and B; Supporting Information Fig. S6A and S6B), lesser time spent in and fewer entries into the open arms in the EPMT (Fig. 5A and B; Fig. S6C) and longer immobility time of mice during the TST and FST compared with FMT-C mice (Fig. 5C). Western blot and IF analysis showed that FMT-M induced a lower expression of SIGMAR1, BDNF, and p-TRKB than those in the FMT-C group (Fig. 5D and E), while the total TRKB was not altered (Fig. 5D). Accordingly, Meth-induced microbial dysbiosis was involved in Meth-related depression and anxiety, while the repression of the SIGMAR1/BDNF/TRKB pathway could be a potential mechanism.
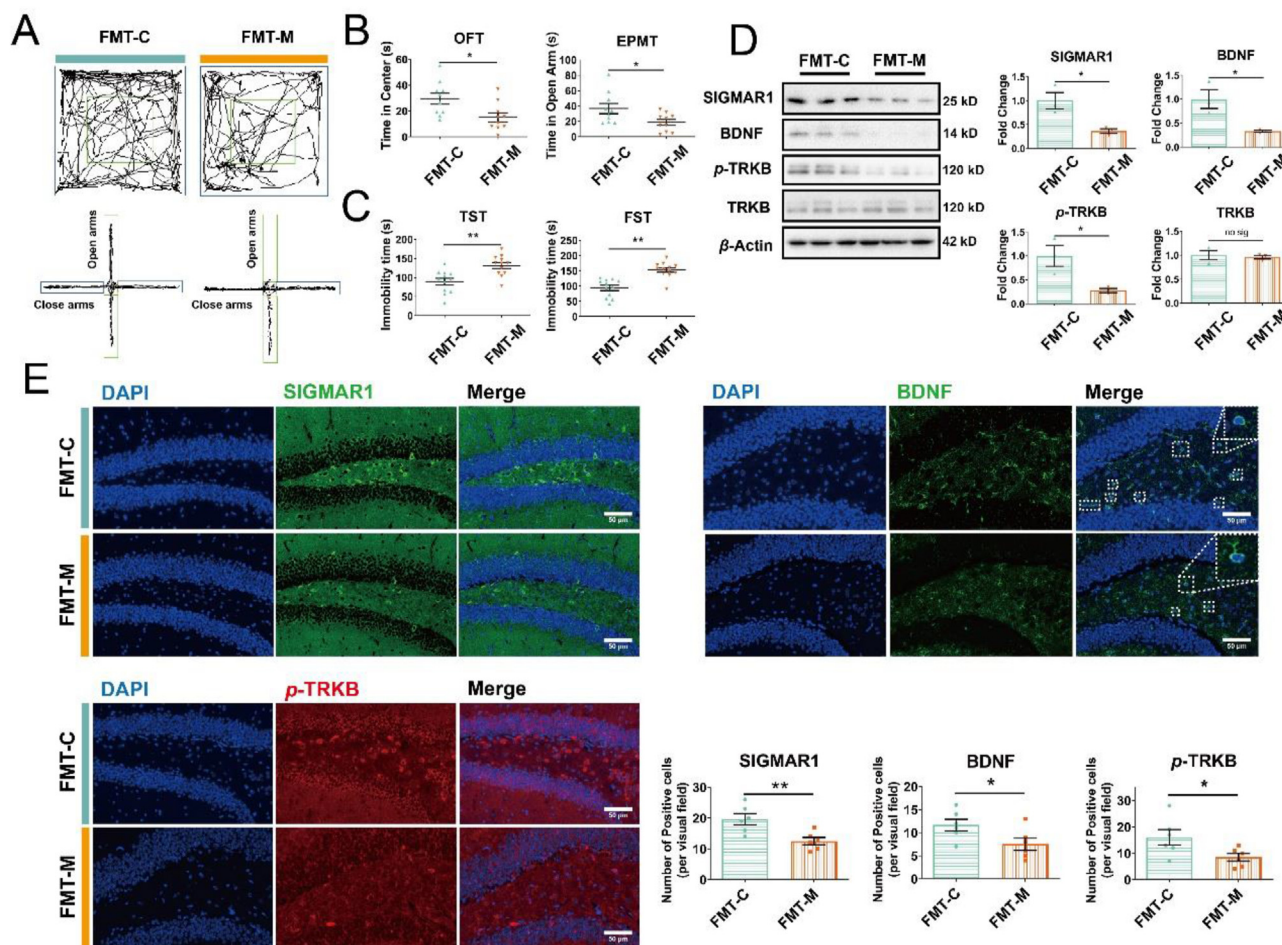
Figure 5 Microbiota from Meth-administrated mice inhibited the SIGMAR1/BDNF/TRKB pathway in the hippocampus and induced anxiety- and depression-like behaviors of recipients. (A) The representative trajectory diagrams in OFT and EPMT. (B) The time the mice spent in the center zone (OFT) and the time the mice spent in open arms (EPMT) ($n = 10$ per group). (C) The total immobility time during the TST and FST ($n = 12$ per group). (D) Protein expressions of SIGMAR1, BDNF, p-TRKB, the total TRKB, and β-actin in FMT-C and FMT-M samples were analyzed by Western blot. β-Actin served as a loading control ($n = 3$ per group). (E) IF staining of SIGMAR1 (in green), BDNF (in green), and p-TRKB (in red) in FMT-C and FMT-M samples. Nuclei were labeled with DAPI (in blue). The number of positive cells is shown ($n = 6$ per group). Scale bar, 50 μm. Data are expressed as mean $\pm$ SEM, $*P < 0.05$, $**P < 0.01$, no sig: no significant difference ($P > 0.05$). All experiments were performed in triplicate at a minimum.

3.4. Microbiota-derived SCFAs attenuated Meth-induced colonic inflammation, and ameliorated the anxiety- and depression-like behaviors

Microbiota-derived SCFAs have emerged the beneficial effects on maintaining intestinal homeostasis and mental disorders[20−23]. Here, acetic and propanoic acids were observed to decrease by Meth. Thus, we added the mixture of acetic and propanoic acids into the drinking-water of mice to investigate its potential protection (Fig. 6A).

3.4.1. Microbiota-derived SCFAs optimized the composition of the gut microbiome and protected against Meth-induced colonic inflammation

Meth initially caused significant weight loss in mice with or without SCFAs supplementation, while SCFAs accelerated its recovery (Fig. 6B). 16S rRNA sequencing revealed the similar OTU abundance or evenness among samples (Supporting Information Fig. S7A). In Alpha diversity, compared to the Saline group, Meth increased the Ace, Chao, and Sobs indexes, while SCFAs supplementation attenuated these alterations (Fig. 6C; Fig. S7B and S7C); meanwhile, there was no significant difference of Simpson and Shannon indexes across groups (Fig. 6C; Fig. S7D), indicating that SCFA could ameliorate Meth-induced increase of microbial richness, and presented no influences on diversity. In Beta diversity, SCFAs dominated the alteration of the principal component in fecal samples, which were further reshaped by Meth administration (Fig. 6D). Furthermore, the abundance of gut microbiota was changed by SCFAs supplementation from Phylum to Genus level (Fig. S7E−S7H). The Sankey diagram further revealed the relative abundance of differential microbiota at the Phylum level and their taxon relationships with differential microbiota at the Genus level in each group (Fig. 6E). At the Genus level, Meth significantly reduced the abundance of nor-ank_f_Muribaculaceae, while SCFAs did not rescue this alteration (Fig. 6F). Meanwhile, SCFAs supplementation ameliorated the Meth-induced increase of Lactobacillus and normalized the abundance of Lachnospiraceae_NK4A136_group, pathogenic
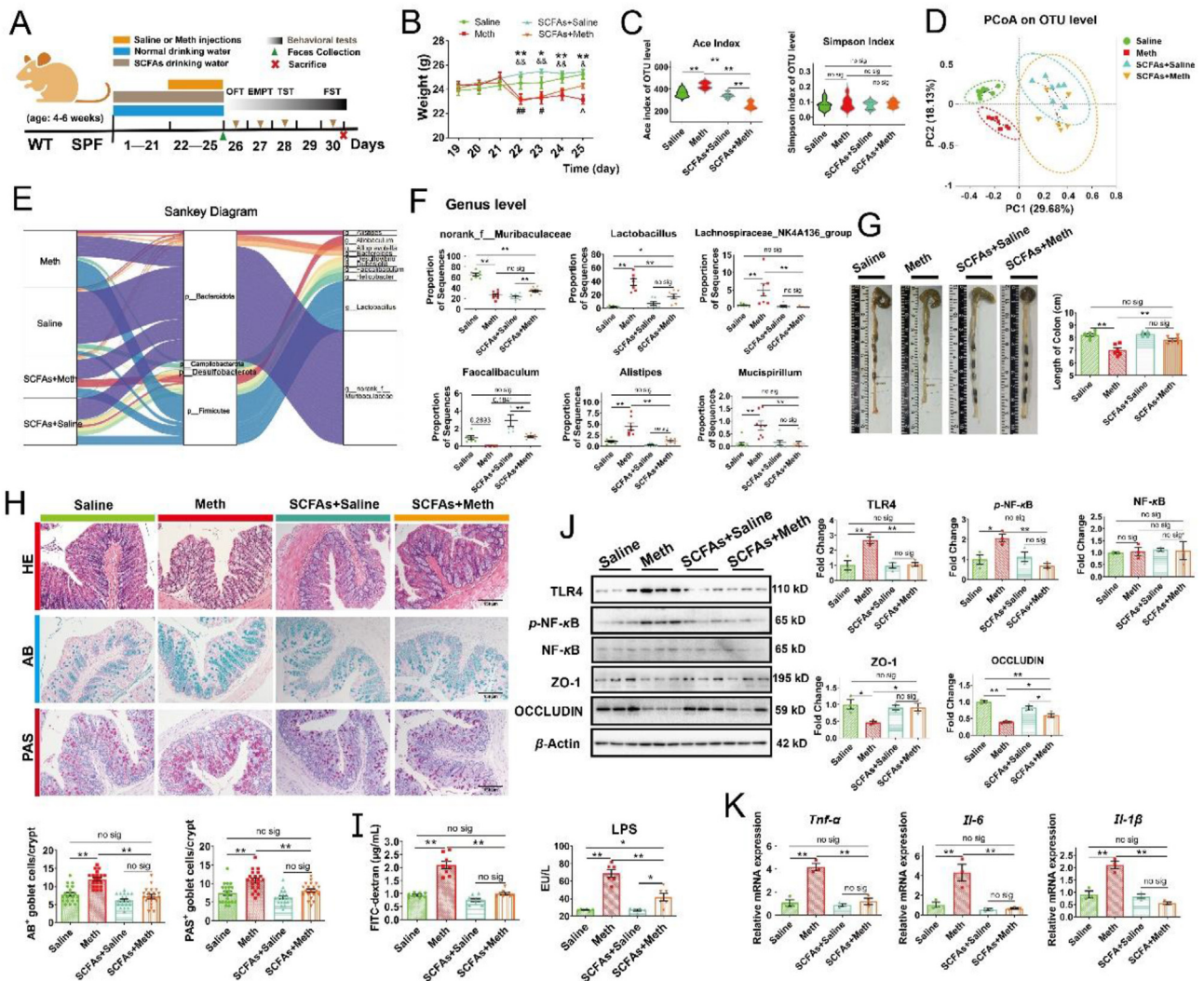
Figure 6 Microbiota-derived SCFAs optimized gut microbiota and protected against Meth-induced colonic inflammation. (A) Schematic diagram of the experimental procedure. (B) Body weight change curves. *$P < 0.05$, **$P < 0.01$ (Meth *vs.* Saline group); #$P < 0.05$, ##$P < 0.01$ (SCFA + Meth *vs.* Saline group); &$P < 0.05$, &&$P < 0.01$ (SCFA + Meth *vs.* SCFA + Saline group); $P < 0.05$, (SCFA + Meth *vs.* Meth group), ($n = 6$ per group). (C) The alteration of alpha diversity at the OTU level: ACE and Simpson indexes ($n = 6-9$ per group). (D) PCoA plot analysis at the OTU level. (E) Sankey diagram: relative abundance of differential microbiota at the Phylum level and the corresponding flows of Genus differential microbiota. The color of the ribbon represented the differential microbiota and its width represented the relative abundance of differential microbiota. (F) The proportion of microbiota sequences at the Genus level across each group. Kruskal−Wallis test with a 95% confidence interval was performed to screen the differential microbiota. (G) The representative images and the colon length across each group ($n = 6$ per group). (H) The representative images of HE, AB, and PAS staining of colonic sections from mice ($n = 6$ per group). The number of AB+ and PAS+ goblet cells per crypt across each group was shown (three random visual fields for each sample) ($n = 20$ per group). Scale bar, 150 μm. (I) The concentration of FITC-dextran ($n = 8$ per group) and LPS ($n = 6$ per group) in serum. (J) Protein expressions of TLR4, p-NF-κB, total NF-κB, ZO-1, OCCLUDIN, and β-actin across each group analyzed by Western blot. β-Actin served as a loading control ($n = 3$ per group). (K) Relative expression of mRNA *Tnf-α*, *Il-6*, and *Il-1β* across each group was normalized by β-actin mRNA ($n = 3$ per group). Data are expressed as mean ± SEM, *$P < 0.05$, **$P < 0.01$, no sig: no significant difference ($P > 0.05$). All experiments were performed in triplicate at a minimum.

Alistipes and Mucispirillum and probiotics Faecalibaculum (Fig. 6F). These results suggested that SCFAs could reshape the gut microbiome and partly normalize Meth-induced microbial disturbance.

Additionally, we observed that SCFAs supplementation prevented Meth-induced shortening of colonic length (Fig. 6G). Correspondingly, SCFAs effectively alleviated Meth-induced enlargement and "balloon-like" changes of goblet cells (Fig. 6H). Further, Meth-induced increase in the number of AB+

and PAS+ goblet cells was also normalized by SCFAs supplementation (Fig. 6H), suggesting that SCFAs could repress Meth-induced excessive proliferation of goblet cells. Additionally, SCFAs presented protective effects on intestinal permeability: Meth induced the elevation of serum FITC-dextran and LPS levels, which were attenuated by SCFAs supplementation (Fig. 6I). In addition, SCFAs effectively attenuated Meth-induced colonic inflammation by inhibiting the activation of the TLR4/NF-κB pathway, evidenced by the lower level of

proteins TLR4 and nuclear p-NF-κB, along with the lower *Tnf-α*, *Il-6*, and *Il-1β* at mRNA level than Meth samples (Fig. 6J and K). Meanwhile, the upregulation of proteins ZO-1 and OCCLUDIN were also observed by SCFAs supplementation relative to the Meth group (Fig. 6J). Thus, our results demonstrated that SCFAs could protect against Meth-induced colonic inflammation and improve intestinal barrier function.

3.4.2. Microbiota-derived SCFAs upregulated the SIGMAR1/BDNF/TRKB pathway and ameliorated Meth-induced anxiety- and depression-like behaviors of mice

Given the beneficial effects of SCFAs on multiple mental disorders, we also explored the regulation of SCFAs on Meth-induced anxiety- and depression disorders. Our results showed that SCFAs effectively mitigated the Meth-induced decrease in depression- and anxiety-like behaviors, demonstrated by the longer total travel distance, more time the mice spent in the center zone, and the decrease of feces amount in OFT (Fig. 7A and B; Supporting

Information Fig. S8A and S8B); the more time mice spent in and the entries into open arms in EPMT (Fig. 7A and B; Fig. S8C); the lesser immobility time in TST and FST than Meth group (Fig. 7C). Moreover, the expression level of SIGMAR1, BDNF, and p-TRKB in Meth-administrated mice was significantly lower than in Saline mice, while SCFA supplementation could alleviate this downregulation (the total TRKB was not altered) (Fig. 7D−F), indicating that SCFAs could rescue Meth-induced inhibition of the SIGMAR1/BDNF/TRKB pathway. Altogether, these results indicated that SCFAs could effectively prevent Meth-induced depression- and anxiety-like behaviors by regulating the SIGMAR1/BDNF/TRKB pathway. Spearman correlation analysis revealed the potential regulation of the microbiota on the colonic damage, IF indexes, and depression- and anxiety-related indicators (Fig. 7G). Specially, the abundance of Faecalibaculum, norank_f_Desulfovibrionaceae, Dubosiella, and Desulfovibrio was strongly positively correlated with the body weight, colonic length, and the expression of SIGMAR1, BDNF, and p-TRKB,

Figure 7 Microbiota-derived SCFAs upregulated the SIGMAR1/BDNF/TRKB pathway in the hippocampus and ameliorated Meth-induced anxiety- and depression-like behaviors. (A) The representative trajectory diagrams in OFT and EPMT. (B) The time the mice spent in the center zone (OFT) and the time the mice spent in the open arms (EPMT) across each group ($n = 10$ per group). (C) The total immobility time across each group during the TST and FST ($n = 12$ per group). (D) Protein expressions of SIGMAR1, BDNF, p-TRKB, the total TRKB, and β-actin across the samples in each group were analyzed by Western blot. β-Actin served as a loading control ($n = 3$ per group). (E) IF staining of SIGMAR1 (in green), BDNF (in green), and p-TRKB (in red) across the Saline, Meth, SCFA + Saline, and SCFA + Meth samples. Nuclei were labeled with DAPI (in blue). Scale bar, 50 μm. (F) The number of positive cells across each group was shown ($n = 6$ per group). (G) Spearman correlation analysis of differential microbiota with colonic, behavioral indicators, and IF. The color of the dots denoted the correlation coefficient and the size of the dots denoted the *P*-value. Red dots represent a positive correlation, while the blue ones represent a negative correlation. Data are expressed as mean ± SEM, $*P < 0.05$, $**P < 0.01$, no sig: no significant difference ($P > 0.05$). All experiments were performed in triplicate at a minimum.
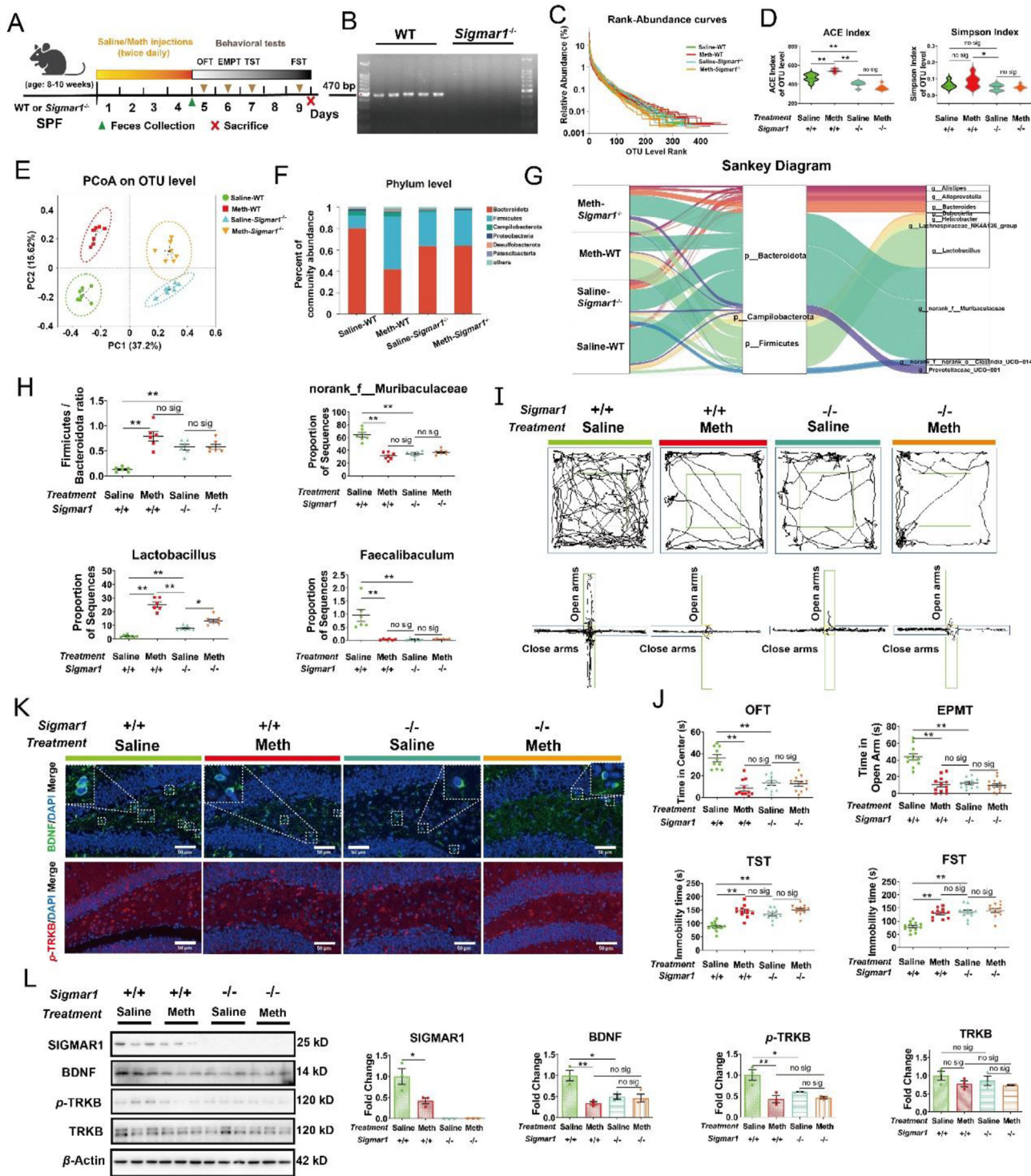
Figure 8 *Sigmar1* knockout disturbed the gut microbiome and resulted in similar behavioral phenotypes with Meth exposure. (A) Schematic diagram of the experimental procedure. (B) Agarose gel electrophoresis of genotype *Sigmar1*. (C) The Rank-Abundance Curves of all samples. (D) The alteration of alpha diversity across the Saline-WT, Meth-WT, Saline-*Sigmar1*$^{-/-}$ and Meth-*Sigmar1*$^{-/-}$ groups, as measured by ACE and Simpson index at the OTU level ($n = 7$ per group). (E) PCoA plot analysis of the Saline-WT (green dots), Meth-WT (red squares), Saline-*Sigmar1*$^{-/-}$ (blue positive triangles), and Meth-*Sigmar1*$^{-/-}$ samples (orange inverted triangles) at the OTU level. (F) Relative abundance of microbiota at the Phylum level. (G) Sankey diagram: relative abundance of differential microbiota at the Phylum level and the corresponding flows of Genus differential microbiota. The color of the ribbon represented the differential microbiota and its width represented the relative abundance of differential microbiota. (H) The ratio of phylum Firmicutes/Bacteroidate across each group ($n = 6$ per group). The proportion of microbiota sequences for genus norank_f_Muribaculaceae, Lactobacillus, and Faecalibaculum across each group ($n = 6–7$ per group). Kruskal−Wallis test with a 95% confidence interval was performed to screen the differential microbiota. (I) The representative trajectory diagrams

while negatively correlated with the number of AB^+ and PAS^+ goblet cells, FD4 level, and the depression- and anxiety-like behaviors. Meanwhile, the abundance of Lactobacillus, Alistipes, Rikenellaceae_RC9_gut_group, Bacteroides, and Roseburia presented a positive correlation with the FD4 level, the number of AB^+ and PAS^+ goblet cells, and the depression- and anxiety-like behaviors, while negatively correlated with the body weight, colonic length, and the expression of SIGMAR1, BDNF, and p-TRKB (Fig. 7G). These suggested that SCFAs-mediated optimization of gut microbiota could participate in its ameliorative effects on Meth-induced colonic damage and behavioral deficits.

Next, we added AA, AP, and their mixture SCFAs into the drinking water of mice respectively to identify which SCFA played a major role in the protective effects (Supporting Information Fig. S9A). In OFT, AA failed to mitigate the Meth-induced decrease in the total travel distance and the time spent in the center zone, and the increase of fecal number (Fig. S9B and S9C). However, Meth-induced deficits of these behavioral indexes (OFT) were effectively attenuated by PA pretreatment and presented no significant difference with the SCFAs + Meth group (Fig. S9B and S9C). In EPMT, the Meth-induced decrease of the time mice spent in open arms was ameliorated by AA, but not PA pretreatment, and both AA and PA significantly alleviated the reduction of the entries mice into open arms (Fig. S9B and S9D). Meanwhile, AA exhibited similar alleviative effects with SCFAs on Meth-induced elevation of immobility time in TST and FST, while the protective effects of PA were not observed (Fig. S9E). Furthermore, the influences of AA, PA, and SCFAs on Meth-induced inhibition of the SIGMAR1/BDNF/TRKB pathway were evaluated. Compared to the Meth group, AA, PA, and SCFAs pretreatment upregulated the expression of proteins SIGMAR1, BDNF, and p-TRKB, while the total TRKB was not altered across the groups. Meanwhile, there was no significant difference in the protein level of SIGMAR1, BDNF, and p-TRKB across the AA + Meth, AP + Meth, and SCFAs + Meth groups (Fig. S9F and S9G). These indicated that the supplementation of AA and PA alone presented the selective improvements of anxiety- and depression-related behavioral indexes, along with the upregulation of SIGMAR1/BDNF/TRKB pathway, while their mixture SCFAs exhibited more comprehensive protection against Meth-related behavioral and neural deficits.

3.5. Sigmar1 knockout disturbed gut microbiome and resulted in similar behavioral phenotypes with Meth exposure by repressing the BDNF/TRKB pathway

Given the regulation of SIGMAR1 on anxiety and depression, the Sigmar1 gene was omitted to investigate its role in Meth-induced mental disorders (Fig. 8A and B).

Interestingly, $Sigmar1^{-/-}$ also presented the regulatory effects on the gut microbiome. Samples among groups showed no significant difference in OTU abundance or evenness (Fig. 8C). In Alpha diversity, $Sigmar1^{-/-}$ mice presented the lower ACE, Chao, and Sobs indexes and Meth failed to increase these indexes, which were

different from the observations in WT mice (Fig. 8D; Supporting Information Fig. S10A and S10B). These indicated the lower richness in $Sigmar1^{-/-}$ mice. Meanwhile, in Simpson and Shannon indexes, there was no significant difference observed between Meth and saline administration in both genotypes (Fig. 8D; Fig. S10C). These indicated that $Sigmar1^{-/-}$ reduced the richness but not the diversity of microbiota. In Beta diversity, PCoA analysis displayed that samples from $Sigmar1^{-/-}$ mice were clearly separated from WT mice, and further clustered according to the saline and Meth administration (Fig. 8E). Additionally, the microbial composition of $Sigmar1^{-/-}$ mice was different from the WT mice irrespective of the Meth administration (Fig. 8F; Fig. S10D−S10F). The relative abundance of differential microbiota at the Phylum level and their taxon relationships with differential microbiota at the Genus level in each group were analyzed using the Sankey diagram (Fig. 8G). Specially, we observed that compared with the Sailne-WT group, $Sigmar1^{-/-}$ induced a higher ratio of phylum Firmicutes/Bacteroidate in mice with or without Meth administration and showed no difference with Meth-WT group (Fig. 8H), suggesting the dysbiosis of the intestinal microenvironment in $Sigmar1^{-/-}$ mice. At the Genus level, Saline-$Sigmar1^{-/-}$ mice presented a lower abundance of norank_f_Muribaculaceae, Faecalibaculum, and higher Lactobacillus compared with Saline-WT mice, which were similar to Meth-induced alterations in WT mice (Fig. 8H). Meanwhile, Meth showed no significant influence in norank_f_Muribaculaceae and Faecalibaculum in $Sigmar1^{-/-}$ mice, while Lactobacillus was further increased (Fig. 8H). Thus, we confirmed that SIGMAR1 participated in the regulation of the gut microbiome.

Next, we determined the alterations of the behavioral phenotypes after Sigmar1 knockout. The results showed that, in WT mice, Meth resulted in a shorter total travel distance, lesser time spent in the center zone, and greater amount of feces in OFT; the lesser time mice spent in and the entries into the open arms in EPMT; the longer immobility time in TST and FST (Fig. 8I and J; Supporting Information Fig. S11A−S11C). Interestingly, these behavioral alterations were also observed in $Sigmar1^{-/-}$ mice without Meth administration (Fig. 8I and J; Fig. S11A−S11C). In addition, after Sigmar1 knockout, the mice exhibited lower BDNF and p-TRKB expression than Saline-WT mice, regardless of Meth administration (Fig. 8K and L; Fig. S11D). These were similar to the effects of Meth on WT mice. Meanwhile, we did not detect the expression of protein SIGMAR1 in $Sigmar1^{-/-}$ mice, confirming its successful knockout (Fig. 8L). These findings suggested the involvement of SIGMAR1 in Meth-induced depression- and anxiety-like behaviors and that its knockout could cause Meth-like behavioral deficits.

3.6. Sigmar1 knockout eliminated the phenotypic differences in anxiety- and depression-like behaviors between FMT-M and FMT-C mice

To explore if FMT-M-induced depression- and anxiety-like behaviors relied on the modulation of SIGMAR1, we transplanted the microbiota from the saline−or Meth-administrated WT mice

in OFT and EPMT. (J) The time the mice spent in the center zone (OFT, $n = 9−12$ per group) and the time the mice spent in open arms across each group (EPMT, $n = 10$ per group). And the total immobility time across each group during the TST and FST ($n = 12$ per group). (K) IF staining of BDNF (in green) and p-TRKB (in red) across the samples in each group. Nuclei were labeled with DAPI (in blue) ($n = 6$ per group). Scale bar, 50 μm. (L) Protein expressions of SIGMAR1, BDNF, p-TRKB, the total TRKB, and β-actin across the samples in each group was analyzed by Western blot. β-Actin served as a loading control ($n = 3$ per group). Data are expressed as mean $\pm$ SEM, $*P < 0.05$, $**P < 0.01$, no sig: no significant difference ($P > 0.05$). All experiments were performed in triplicate at a minimum.

into the *Sigmar1*$^{-/-}$ mice (Fig. 9A). In behavioral tests, compared with the FMT-C-WT group, FMT-C-*Sigmar1*$^{-/-}$ induced depression- and anxiety-like behaviors, which was demonstrated by the shorter total travel distance, the lesser time spent in the center zone and the greater amount of feces in OFT, the lesser time the mice spent and the fewer entries into the open arms in EPMT, and

the longer immobility time in TST and FST (Fig. 9B and C; Supporting Information Fig. S12A−S12C). These suggested that the FMT-M-induced behavioral differences from FMT-C in WT mice were leveled out by *Sigmar1* knockout. Additionally, FMT-C-*Sigmar1*$^{-/-}$ displayed a lower level of BDNF and p-TRKB than the FMT-C-WT mice and showed no significant
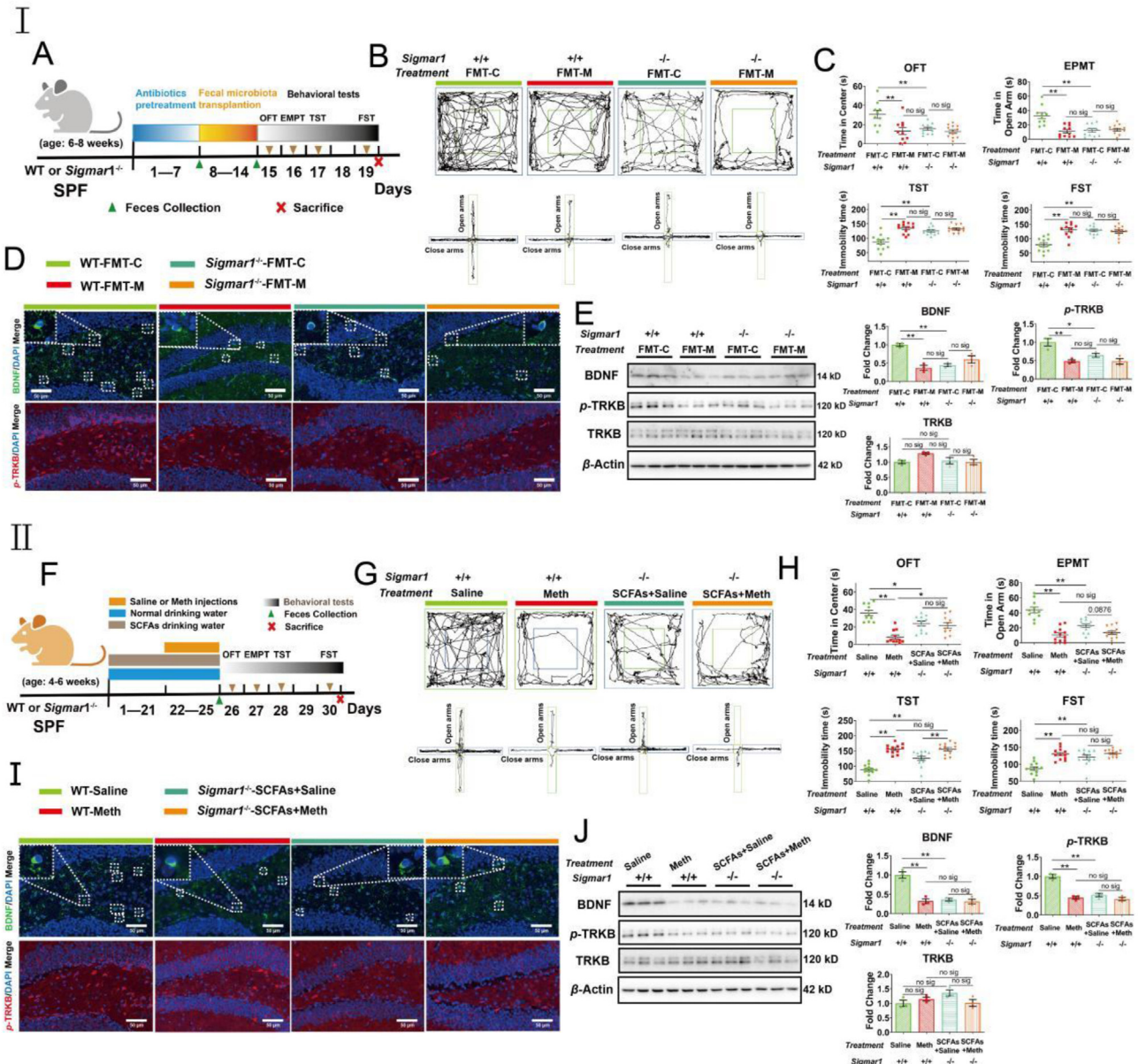

Figure 9 I) *Sigmar1* knockout eliminated the phenotypic differences in behaviors between FMT-M and FMT-C mice. (A) Schematic diagram of the experimental procedure. (B) The representative trajectory diagrams in OFT and EPMT. (C) The time the mice spent in the center zone (OFT, $n = 10−11$ per group) and the time the mice spent in open arms across each group (EPMT, $n = 10−12$ per group). The total immobility time across each group during TST and FST. $n = 12$ per group. (D) IF staining of BDNF (in green) and p-TRKB (in red) across the samples in each group. Nuclei were labeled with DAPI (in blue) ($n = 6$ per group). Scale bar, 50 μm. (E) Protein expressions of BDNF, p-TRKB, the total TRKB, and β-actin across the samples in each group were analyzed by Western blot. β-Actin served as a loading control ($n = 3$ per group). II) *Sigmar1* knockout eliminated the protective effects of SCFAs on Meth-induced depression- and anxiety-like behaviors. (F) Schematic diagram of the experimental procedure. (G) The representative trajectory diagrams in OFT and EPMT. (H) The time the mice spent in the center zone (OFT, $n = 10−11$ per group) and the time mice spent in the open arms (EPMT, $n = 10−12$ per group) across each group. The total immobility time across each group during TST and FST ($n = 12$ per group). (I) IF staining of BDNF (in green) and p-TRKB (in red) across the samples in each group. Nuclei were labeled with DAPI (in blue) ($n = 6$ per group). Scale bar, 50 μm. (J) Protein expressions of BDNF, p-TRKB, the total TRKB, and β-actin across the samples in each group was analyzed by Western blot. β-Actin served as a loading control ($n = 3$ per group). Data are expressed as mean ± SEM, *$P < 0.05$, **$P < 0.01$, no sig: no significant difference ($P > 0.05$). All experiments were performed in triplicate at a minimum.

difference with the FMT-M-*Sigmar1*$^{-/-}$ mice (Fig. 9D and E; Fig. S12D and S12E). These results suggested that the regulation of the gut microbiota on depression and anxiety relied on the modulation of the SIGMAR1/BDNF/TRKB pathway.
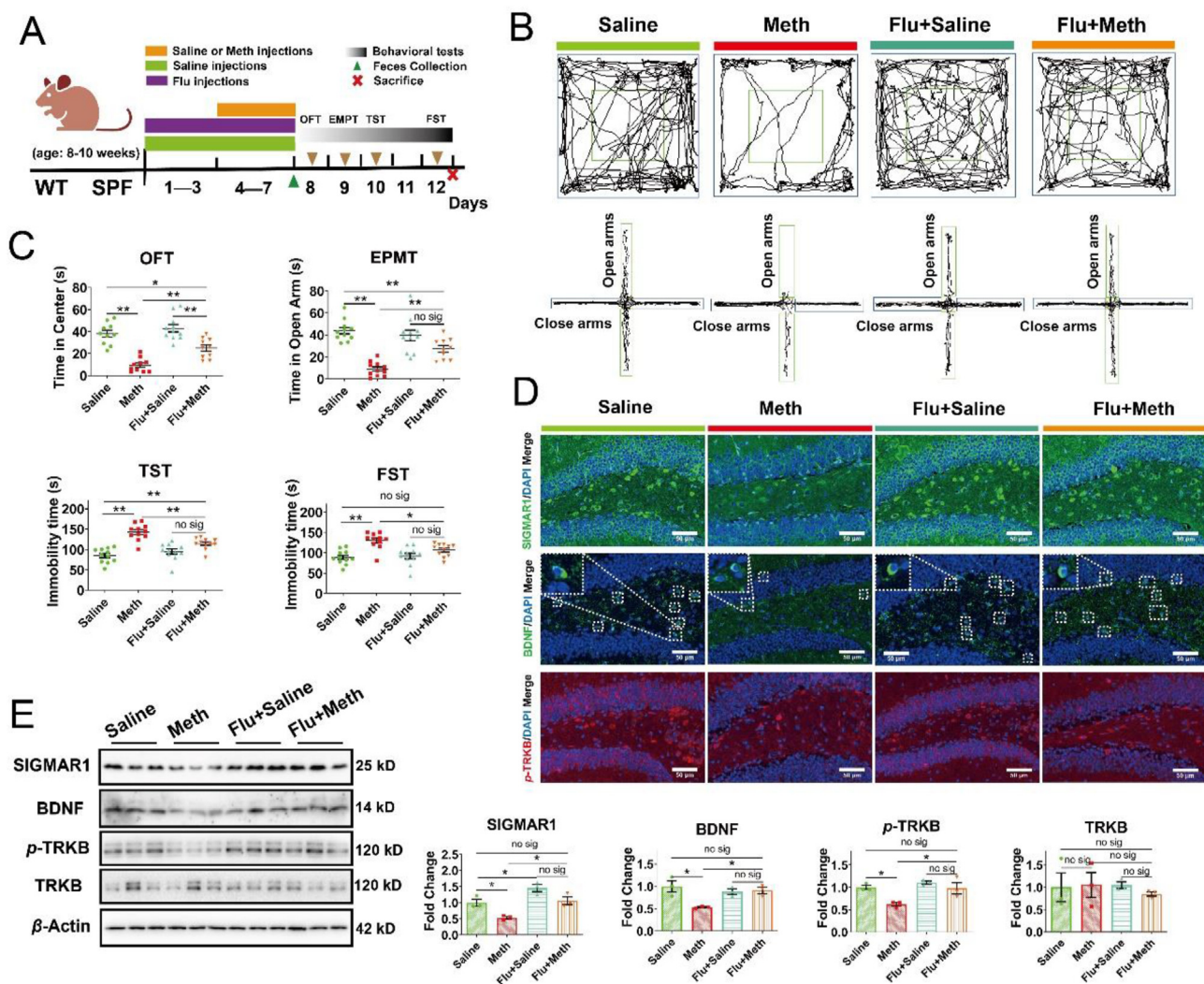
3.7. Sigmar1 knockout abolished the protective effects of SCFAs on Meth-induced anxiety- and depression-like behaviors by suppressing the BDNF/TRKB pathway

Next, we investigated the role of SIGMAR1 in the protection of SCFAs on Meth-induced mental disorders (Fig. 9F). Behavioral tests showed that there was no significant difference in depression- and anxiety-related indicators between the SCFA-Meth-*Sigmar1*$^{-/-}$ and Meth-WT groups, except for the time spent in the center zone (OFT) (Fig. 9G and H; Supporting Information Fig. S13A−S13C),

suggesting that SCFAs failed to mitigate Meth-induced depression- and anxiety-like behaviors after *Sigmar1* knockout. Moreover, SCFAs failed to attenuate the Meth-induced decrease of BDNF and p-TRKB in *Sigmar1*$^{-/-}$ mice (Fig. 9I and J; Fig. S13D and S13E), which were different from the observations in WT mice. Thus, our results indicated that the protective effects of SCFAs on Meth-induced depression- and anxiety-like behaviors were dependent on the modulation of the SIGMAR1/BDNF/TRKB pathway.

3.8. Fluvoxamine, an agonist of SIGMAR1, alleviated Meth-induced anxiety- and depression-like behaviors by activating the SIGMAR1/BDNF/TRKB pathway

To verify the protection of SIGMAR1 on Meth-induced mental disorders, Flu was utilized to activate the SIGMAR1 (Fig. 10A). In

Figure 10 Fluvoxamine ameliorated Meth-induced anxiety- and depression-like behaviors by stimulating the SIGMAR1/BDNF/TRKB pathway. (A) Schematic diagram of the experimental procedure. (B) The representative trajectory diagrams in OFT and EPMT. (C) The time the mice spent in the center zone (OFT, $n = 10-12$ per group) and the time the mice spent in open arms (EPMT, $n = 10-11$ per group) across each group. The total immobility time across each group during TST and FST ($n = 11$ per group). (D) IF staining of SIGMAR1 (in green), BDNF (in green), and p-TRKB (in red) across the Saline, Meth, Flu + Saline, and Flu + Meth samples. Nuclei were labeled with DAPI (in blue) ($n = 6$ per group). Scale bar, 50 μm. (E) Protein expressions of SIGMAR1, BDNF, p-TRKB, the total TRKB, and β-actin across the samples in each group was analyzed by Western blot. β-Actin served as a loading control ($n = 3$ per group). Data are expressed as mean ± SEM, *$P < 0.05$, **$P < 0.01$, no sig: no significant difference ($P > 0.05$). All experiments were performed in triplicate at a minimum.

behavioral tests, we observed that the Meth-induced depression- and anxiety-like behaviors were also attenuated by Flu treatment, as demonstrated by the longer total travel distance, the more time spent in the center zone, and the lower amount of feces in OFT, the longer time the mice spent and the more entries into the open arms in EPMT, and the shorter immobility time in TST and FST after Flu treatment compared with the Meth group (Fig. 10B and C; Supporting Information Fig. S14A−S14C). Furthermore, compared to the Saline group, we observed that we observed that Flu overexpressed the level of SIGMAR1 in both saline- and Meth-administrated mice and attenuated the Meth-induced downregulation of BDNF and p-TRKB (Fig. 10D and E; Fig. S14D). These observations further confirmed the protective effects of SIGMAR1 on Meth-induced depression- and anxiety-like behaviors.

Next, we profiled the alteration of gut microbiome after Flu treatment. Rank-Abundance curves presented similar OTU abundance or evenness among all samples (Supporting Information Fig. S15A). In Alpha diversity, Meth induced a higher ACE index than the Saline group, while this alteration was mitigated by Flu treatment (Fig. S15B). Meanwhile, there was no significant difference between the Saline and Meth groups, while Flu + Meth resulted in the elevation of the Simpson index relative to the Saline group (Fig. S15B). These suggested that Flu could ameliorate the Meth-induced richness of microbiota and induce a higher microbial diversity. In Beta diversity, we observed that the principal composition of fecal samples in the Saline group was separated from the Meth group, and Flu altered the sample composition of both groups (Fig. S15C). Moreover, the abundance of gut microbiota from Phylum to Genus level was altered by Flu treatment (Fig. S15D−S15F). The differential microbiota from Phylum to Genus level were further summarized using the LEfSe cladogram (Fig. S15G). In addition, the concentration of SCFAs in Flu-treated fecal samples was also determined (Fig. S15H). Interestingly, mice treated with Flu showed a much higher level of acetic acid, hexanoic acid, and isohexanoic acid than those without Flu treatment, regardless of Meth administration (Fig. S15H). Meanwhile, Flu attenuated the Meth-induced decrease of propanoic acid, while the lowered isobutyric acid and isovaleric acid level was not effectively alleviated by Flu treatment. And there was no significant difference in the concentration of Butanoic acid and Valeric acid across the groups (Fig. S15H). These results indicated that Flu treatment could reshape Meth-induced disturbance of gut microbiota and partly ameliorate the decrease of fecal SCFAs. Moreover, we explored the influences of Flu on the level of serum SCFAs. The results showed that Meth led to a decrease in serum acetic acid, propanoic acid, and hexanoic acid compared to the Saline group, while Flu treatment did not mitigate these changes (Fig. S15I). Additionally, there were no significant differences in the levels of serum butanoic acid, valeric acid, isobutyric acid, and isovaleric acid across the groups (Fig. S15I). As for the level of isohexanoic acid, the Flu + Meth group exhibited a lower concentration than the Saline group (Fig. S15I). These observations suggested that Flu exerted only a weak regulatory influence on Meth-induced alterations in serum SCFAs composition.

Finally, to investigate the role of microbiota in Flu-mediated protective effects, mice were orally pretreated with fecal microbiota from Flu-treated mice before Meth challenges (Supporting Information Fig. S16A). Behavioral results showed that in OFT, there was no significant difference in the total travel distance, time mice spent in the center zone, and the fecal number between the FMT-Flu + Meth and PBS + Meth groups (Fig. S16B and S16C).

In EPMT, gut microbiota from Flu-treated mice failed to ameliorate Meth-induced decrease in the time mice spent in and the entries into open arms (Fig. S16B and S16D). Meanwhile, in TST and FST, FMT-Flu + Meth also presented no significant difference in immobility time with the PBS + Meth group (Fig. S16E). In addition, gut microbiota from Flu-treated mice also failed to attenuate Meth-induced repression of the SIGMAR1/BDNF/TRKB pathway. FMT-Flu + Meth resulted in a lower level of proteins SIGMAR1, BDNF, and p-TRKB in comparison with the PBS + Saline group and presented no significant difference with the PBS + Meth group (Fig. S16F and S16G). These findings suggested that Flu-induced alteration of gut microbiota did not contribute to the protective effects of Flu on Meth-induced depression- and anxiety-like behaviors, and the upregulation of the SIGMAR1/BDNF/TRKB pathway.

4. Discussion

Gut microbiota is a crucial contributor to maintaining the host health[57]. Its-derived SCFAs are recognized as the important mediums of gut microbiota to regulate the gut immune and to influence the mental health of the host[20−23]. In this study, the inflammation-related TLR4/NF-κB pathway was significantly enriched after Meth administration based on RNA-seq. Meanwhile, the anti-inflammatory bacterium Faecalibaculum[58] was also lowered by Meth, implying that microbial dysbiosis could participate in Meth-induced colonic inflammation. Correspondingly, we observed that gut microbiota from Meth-administrated mice also aroused the TLR4-related colonic inflammation and caused the dysfunction of the intestinal barrier in recipients. TLR4 is a member of the TLR family inducing pro-inflammation response and can be activated by LPS (the component of Gram-negative bacteria)[59], while the pro-inflammatory effect of microbial dysbiosis is the important avenue to impair the intestinal barrier function[60]. The higher serum LPS level was also observed after FMT-M administration. Moreover, the decrease in SCFAs could be a trigger factor for these consequences. In fact, SCFAs can serve as ligands for G-protein coupled receptors, which further activate anti-inflammatory signaling cascades[61,62]. Additionally, SCFAs have emerged with the capacity of improving the intestinal mucosal barrier[62]. Indeed, SCFAs supplementation effectively ameliorated Meth-induced colonic inflammation by suppressing the TLR4/NF-κB pathway and strengthening the intestinal barrier. These findings confirmed that gut microbiota participated in Meth-induced impairment of intestinal homeostasis, which could be mitigated by SCFAs. Furthermore, accumulating evidence suggests that there exhibited complex interactions between colonic inflammation and mental disorders, including depression and anxiety[63]. Patients with inflammatory bowel disease experienced a higher risk of depression and anxiety. And in experimental models of colitis, rodents also presented strong depression- and anxiety-like behaviors[64−66]. Accompanied by the colonic inflammation, Meth also caused depression- and anxiety-like behaviors in mice, implying that colonic inflammation could contribute to Meth-related mental disorders. Additionally, behavioral phenotypes of depression and anxiety in inflammatory bowel disease patients could be transferred to the recipient mice by fecal microbiota transplantation[67]. Here, the FMT experiment reproduced Meth-induced depression- and anxiety-like behaviors in recipients, suggesting that gut microbiota could serve as the linker between Meth-related colonic inflammation and mental disorders.

Notably, Meth induced opposed alterations of mainly SCFAs producers: the downregulated Muribaculaceae and upregulated Lactobacillaceae[68]. We speculated that it could involve in the microbial mechanism of rescue. Muribaculaceae was the dominant bacteria and its downregulation reduced the SCFAs level, while the increased Lactobacillaceae failed to reverse it. Correspondingly, SCFAs supplementation normalized the abundance of Lactobacillaceae and repressed the recovery of Muribaculaceae, which prevented the overproduction of SCFAs. In addition, probiotic Lactobacillaceae can promote the proliferation of goblet cells to improve the function of the intestinal barrier[69,70]. Here, accompanied by the upregulated Lactobacillaceae, we also observed the excessive proliferation of goblet cells after Meth administration, although the barrier function was not ameliorated.

In addition, Meth-induced anxiety- and depression-like behaviors were transferred to the recipients through fecal microbiota transplant, indicating the involvement of microbiota in Meth-induced anxiety and depression. An increasing body of evidence presented the regulatory effects of gut microbiota on mental disorders[9−11]. Gut microbiota was observed disordered in depression patients, and its transplant induced depression-like behavior of germ-free mice[10,12]. Even gene-mediated anti-anxiety and -depression phenotypes could be transferred through fecal microbiota transplant[71]. Furthermore, accompanied by these behavioral phenotypes, we observed the repression of the SIGMAR1/BDNF/TRKB pathway both after Meth and FMT-M administration, implying its potential regulation of behavioral deficits. In fact, the pharmacological activation of SIGMAR1 has been recognized as an effective therapeutic strategy for anxiety and depression in clinic[33]. Meanwhile, its downstream BDNF and TRKB are also the key molecules for anti-anxiety and -depression[35], which could be modulated by gut microbiota[72,73]. Further, through Sigmar1 knockout and activation, we verified that Meth-induced anxiety and depression relied on the inhibition of SIGMAR1/BDNF/TRKB pathway. In parallel, Sigmar1 knockout eliminated microbiota-induced differences in behavioral phenotypes, confirming that SIGMAR1 mediated microbiota-induced anxiety- and depression-like behaviors. Additionally, we observed that Sigmar1 knockout also disturbed the gut microbiome. In our previous study, gut microbiota from Sigmar1 knockout mice also partly reproduced genotype-related depression- and anxiety-like behaviors[74]. These suggested that there existed a dynamic balance between gut microbiota and SIGMAR1, and gut microbiota could contribute to the modulation of SIGMAR1 on behaviors.

In this study, we observed a decrease in microbiota-derived SCFAs, both in feces and serum, due to Meth administration. Supplementation with SCFAs alleviated Meth-induced depression- and anxiety-like behaviors, potentially through regulation of the SIGMAR1/BDNF/TRKB pathway. Through oral supplementation, SCFAs could regulate the homeostasis of colonic Treg cells[75], suggesting that oral SCFAs supplementation could transit through the small intestine and act on the colonic tissue. Meanwhile, both oral SCFAs supplementation and microbial colonization could improve microbial knockout-induced deficiency of microglia in the brain[76], indicating that gut microbiota and its derivation SCFAs played a crucial role in modulating neural function. In fact, the protective effects of SCFAs were observed in diet-related depression[77] and even in chronic cerebral hypoperfusion-induced depression[78]. SCFAs also presented the alleviative effects on innate anxiety[79] and the anti-anxiety effects of prebiotics strongly correlated with gut SCFAs level[25]. In addition, SCFAs failed to ameliorate Meth-induced anxiety and depression in Sigmar1$^{−/−}$ mice, indicating that the protective effects of SCFAs against Meth-

induced mental disorders were dependent on the modulation of SIGMAR1.

By activating the SIGMAR1, Flu upregulated the BDNF/TRKB pathway and ameliorated Meth-induced depression- and anxiety-like behaviors. This further confirmed that Meth-induced mental disorders relied on its repression of SIGMAR1. Interestingly, we also observed that Flu treatment reshaped Meth-induced microbial disturbance and partly attenuated Meth-induced decrease of SCFAs, implying that gut microbiota could participate in the protective effects of Flu. However, gut microbiota from Flu-treated mice failed to alleviate Meth-induced inhibition of the SIGMAR1/BDNF/TRKB pathway and showed no effective protection against depression- and anxiety-like behaviors. Flu exhibited a limited regulatory effect on Meth-induced alterations in serum SCFAs. These findings suggest that the gut microbiota-mediated short-term elevation of fecal SCFAs was insufficient to counteract the Meth-induced decrease in serum SCFAs or to alleviate associated mental disorders (as the SCFAs supplementation experiment lasted three weeks). Furthermore, Flu exerted its antidepressant and anxiolytic effects primarily by directly targeting SIGMAR1.

However, there are still a few shortcomings of this study to be noted. Here, the detailed mechanisms of how SCFAs modulate Meth-induced anxiety and depression disorders are still unclear, especially the potential regulation of free fatty acid receptor on SIGMAR1. Another shortcoming is that our study only focused on the protective effects of acetic acid and propanoic acid, while the role of other SCFAs needs to be further clarified.

5. Conclusions

Our findings indicate that gut microbiota participated in Meth-induced colonic inflammation and contributed to Meth-related anxiety and depression disorders; microbiota-derived SCFAs could optimize gut homeostasis and protect against Meth-induced anxiety and depression in SIGMAR1 dependent manner. Overall, this study revealed the microbial mechanisms of Meth-induced anxiety and depression disorders and provided a potential candidate in therapeutic strategy.

Data availability

The data used to support the findings of this study have been deposited in the NCBI Sequence Read Archive under accession no. PRJNA878621, PRJNA879093 and PRJNA967461. The Raw images of Western blots from all Figures are shown in Supporting Information Fig. S17.

Acknowledgments

Author contributions

Qi Wang and Xiaoli Xie contributed to conception and design of the study. Kaikai Zhang and Lijian Chen organized the database. Jianzheng Yang, Yi Liu and Xiuwen Li performed the statistical analysis. Kaikai Zhang and Jiali Liu wrote the first draft of the

manuscript. Jiahao Li, Long Chen, Clare Hsu and Jiahao Zeng, wrote sections of the manuscript. All authors contributed to manuscript revision, read, and approved the submitted version.

Conflicts of interest

The authors declare no conflicts of interest.

Appendix A.   Supporting information

Supporting data to this article can be found online at https://doi.org/10.1016/j.apsb.2023.09.010.

References

1. Homer BD, Solomon TM, Moeller RW, Mascia A, Deraleau L, Halkitis PN. Methamphetamine abuse and impairment of social functioning: a review of the underlying neurophysiological causes and behavioral implications. *Psychol Bull* 2008;**134**:301−10.
2. Zhang KK, Liu JL, Chen LJ, Li JH, Yang JZ, Xu LL, et al. Gut microbiota mediates methamphetamine-induced hepatic inflammation *via* the impairment of bile acid homeostasis. *Food Chem Toxicol* 2022;**166**:113208.
3. Zhao J, Ying L, Liu Y, Liu N, Tu G, Zhu M, et al. Different roles of Rac1 in the acquisition and extinction of methamphetamine-associated contextual memory in the nucleus accumbens. *Theranostics* 2019;**9**:7051−71.
4. Howells FM, Temmingh HS, Hsieh JH, van Dijen AV, Baldwin DS, Stein DJ. Electroencephalographic delta/alpha frequency activity differentiates psychotic disorders: a study of schizophrenia, bipolar disorder and methamphetamine-induced psychotic disorder. *Transl Psychiatry* 2018;**8**:75.
5. Kim B, Tag SH, Nam E, Ham S, Ahn S, Kim J, et al. SYNCRIP controls miR-137 and striatal learning in animal models of methamphetamine abstinence. *Acta Pharm Sin B* 2022;**12**:3281−97.
6. Chen XJ, Wang CG, Liu W, Gorowska M, Wang DM, Li YH. Identification of the features of emotional dysfunction in female individuals with methamphetamine use disorder measured by musical stimuli modulated startle reflex. *Front Hum Neurosci* 2018;**12**:230.
7. Glasner-Edwards S, Mooney LJ. Methamphetamine psychosis: epidemiology and management. *CNS Drugs* 2014;**28**:1115−26.
8. Simpson CA, Diaz-Arteche C, Eliby D, Schwartz OS, Simmons JG, Cowan C. The gut microbiota in anxiety and depression—a systematic review. *Clin Psychol Rev* 2021;**83**:101943.
9. Li N, Wang Q, Wang Y, Sun A, Lin Y, Jin Y, et al. Fecal microbiota transplantation from chronic unpredictable mild stress mice donors affects anxiety-like and depression-like behavior in recipient mice *via* the gut microbiota−inflammation−brain axis. *Stress* 2019;**22**:592−602.
10. Zheng P, Zeng B, Zhou C, Liu M, Fang Z, Xu X, et al. Gut microbiome remodeling induces depressive-like behaviors through a pathway mediated by the host's metabolism. *Mol Psychiatr* 2016;**21**:786−96.
11. Kelly JR, Borre Y, O BC, Patterson E, El AS, Deane J, et al. Transferring the blues: depression-associated gut microbiota induces neurobehavioural changes in the rat. *J Psychiatr Res* 2016;**82**:109−18.
12. Nikolova VL, Smith M, Hall LJ, Cleare AJ, Stone JM, Young AH. Perturbations in gut microbiota composition in psychiatric disorders: a review and meta-analysis. *JAMA Psychiatr* 2021;**78**:1343−54.
13. Diaz HR, Wang S, Anuar F, Qian Y, Björkholm B, Samuelsson A, et al. Normal gut microbiota modulates brain development and behavior. *Proc Natl Acad Sci U S A* 2011;**108**:3047−52.
14. Needham BD, Funabashi M, Adame MD, Wang Z, Boktor JC, Haney J, et al. A gut-derived metabolite alters brain activity and anxiety behaviour in mice. *Nature* 2022;**602**:647−53.
15. Gao K, Mu CL, Farzi A, Zhu WY. Tryptophan metabolism: a link between the gut microbiota and brain. *Adv Nutr* 2020;**11**:709−23.
16. Mayer EA, Tillisch K, Gupta A. Gut/brain axis and the microbiota. *J Clin Invest* 2015;**125**:926−38.
17. Morais LH, Schreiber HT, Mazmanian SK. The gut microbiota−brain axis in behaviour and brain disorders. *Nat Rev Microbiol* 2021;**19**:241−55.
18. Cryan JF, O'Riordan KJ, Cowan C, Sandhu KV, Bastiaanssen T, Boehme M, et al. The microbiota−gut−brain axis. *Physiol Rev* 2019;**99**:1877−2013.
19. Zhang ZW, Gao CS, Zhang H, Yang J, Wang YP, Pan LB, et al. *Morinda officinalis* oligosaccharides increase serotonin in the brain and ameliorate depression *via* promoting 5-hydroxytryptophan production in the gut microbiota. *Acta Pharm Sin B* 2022;**12**:3298−312.
20. Lu H, Xu X, Fu D, Gu Y, Fan R, Yi H, et al. Butyrate-producing *Eubacterium rectale* suppresses lymphomagenesis by alleviating the TNF-induced TLR4/MyD88/NF-κB axis. *Cell Host Microbe* 2022;**30**:1139−50.
21. Ezzine C, Loison L, Montbrion N, Bôle-Feysot C, Déchelotte P, Coëffier M, et al. Fatty acids produced by the gut microbiota dampen host inflammatory responses by modulating intestinal SUMOylation. *Gut Microb* 2022;**14**:2108280.
22. Erny D, Dokalis N, Mezö C, Castoldi A, Mossad O, Staszewski O, et al. Microbiota-derived acetate enables the metabolic fitness of the brain innate immune system during health and disease. *Cell Metabol* 2021;**33**:2260−76.
23. Dalile B, Van Oudenhove L, Vervliet B, Verbeke K. The role of short-chain fatty acids in microbiota−gut−brain communication. *Nat Rev Gastroenterol Hepatol* 2019;**16**:461−78.
24. Lee J, Venna VR, Durgan DJ, Shi H, Hudobenko J, Putluri N, et al. Young *versus* aged microbiota transplants to germ-free mice: increased short-chain fatty acids and improved cognitive performance. *Gut Microb* 2020;**12**:1−14.
25. Burokas A, Arboleya S, Moloney RD, Peterson VL, Murphy K, Clarke G, et al. Targeting the microbiota−gut−brain axis: prebiotics have anxiolytic and antidepressant-like effects and reverse the impact of chronic stress in mice. *Biol Psychiatr* 2017;**82**:472−87.
26. Huang W, Hu W, Cai L, Zeng G, Fang W, Dai X, et al. Acetate supplementation produces antidepressant-like effect *via* enhanced histone acetylation. *J Affect Disord* 2021;**281**:51−60.
27. Ning T, Gong X, Xie L, Ma B. Gut microbiota analysis in rats with methamphetamine-induced conditioned place preference. *Front Microbiol* 2017;**8**:1620.
28. Yang C, Fu X, Hao W, Xiang X, Liu T, Yang BZ, et al. Gut dysbiosis associated with the rats' responses in methamphetamine-induced conditioned place preference. *Addiction Biol* 2021;**26**:e12975.
29. Martin P, Reeder T, Sourbron J, de Witte P, Gammaitoni AR, Galer BS. An emerging role for sigma-1 receptors in the treatment of developmental and epileptic encephalopathies. *Int J Mol Sci* 2021;**22**:8416.
30. Hindmarch I, Hashimoto K. Cognition and depression: the effects of fluvoxamine, a sigma-1 receptor agonist, reconsidered. *Hum Psychopharmacol* 2010;**25**:193−200.
31. Wu NH, Ye Y, Wan BB, Yu YD, Liu C, Chen QJ. Emerging benefits: pathophysiological functions and target drugs of the sigma-1 receptor in neurodegenerative diseases. *Mol Neurobiol* 2021;**58**:5649−66.
32. Wang Y, Gao C, Gao T, Zhao L, Zhu S, Guo L. Plasma exosomes from depression ameliorate inflammation-induced depressive-like behaviors *via* sigma-1 receptor delivery. *Brain Behav Immun* 2021;**94**:225−34.
33. Gothelf D, Rubinstein M, Shemesh E, Miller O, Farbstein I, Klein A, et al. Pilot study: fluvoxamine treatment for depression and anxiety disorders in children and adolescents with cancer. *J Am Acad Child Adolesc Psychiatry* 2005;**44**:1258−62.
34. Hashimoto K. Sigma-1 receptor chaperone and brain-derived neurotrophic factor: emerging links between cardiovascular disease and depression. *Prog Neurobiol* 2013;**100**:15−29.
35. Martinowich K, Manji H, Lu B. New insights into BDNF function in depression and anxiety. *Nat Neurosci* 2007;**10**:1089−93.
36. Sambo DO, Lin M, Owens A, Lebowitz JJ, Richardson B, Jagnarine DA, et al. The sigma-1 receptor modulates methamphetamine dysregulation of dopamine neurotransmission. *Nat Commun* 2017;**8**:2228.

37. Xie XL, He JT, Wang ZT, Xiao HQ, Zhou WT, Du SH, et al. Lactulose attenuates METH-induced neurotoxicity by alleviating the impaired autophagy, stabilizing the perturbed antioxidant system and suppressing apoptosis in rat striatum. *Toxicol Lett* 2018;**289**:107−13.

38. Tan XH, Zhang KK, Xu JT, Qu D, Chen LJ, Li JH, et al. Luteolin alleviates methamphetamine-induced neurotoxicity by suppressing PI3K/Akt pathway-modulated apoptosis and autophagy in rats. *Food Chem Toxicol* 2020;**137**:111179.

39. Melega WP, Cho AK, Harvey D, Laćan G. Methamphetamine blood concentrations in human abusers: application to pharmacokinetic modeling. *Synapse* 2007;**61**:216−20.

40. Wang Q, Wei LW, Xiao HQ, Xue Y, Du SH, Liu YG, et al. Methamphetamine induces hepatotoxicity *via* inhibiting cell division, arresting cell cycle and activating apoptosis: *in vivo* and *in vitro* studies. *Food Chem Toxicol* 2017;**105**:61−72.

41. Li Y, Luo ZY, Hu YY, Bi YW, Yang JM, Zou WJ, et al. The gut microbiota regulates autism-like behavior by mediating vitamin B$_6$ homeostasis in EphB6-deficient mice. *Microbiome* 2020;**8**:120.

42. Erny D, Hrabĕ DAA, Jaitin D, Wieghofer P, Staszewski O, David E, et al. Host microbiota constantly control maturation and function of microglia in the CNS. *Nat Neurosci* 2015;**18**:965−77.

43. Smith PM, Howitt MR, Panikov N, Michaud M, Gallini CA, Bohlooly YM, et al. The microbial metabolites, short-chain fatty acids, regulate colonic Treg cell homeostasis. *Science* 2013;**341**:569−73.

44. Normann C, Frase S, Haug V, von Wolff G, Clark K, Münzer P, et al. Antidepressants rescue stress-induced disruption of synaptic plasticity *via* serotonin transporter-independent inhibition of L-type calcium channels. *Biol Psychiatr* 2018;**84**:55−64.

45. Wu Z, Huang S, Li T, Li N, Han D, Zhang B, et al. Gut microbiota from green tea polyphenol-dosed mice improves intestinal epithelial homeostasis and ameliorates experimental colitis. *Microbiome* 2021;**9**:184.

46. Tang C, Wang Q, Shen J, Wang C, Ding H, Wen S, et al. Neuron stem cell NLRP6 sustains hippocampal neurogenesis to resist stress-induced depression. *Acta Pharm Sin B* 2023;**13**:2017−38.

47. Yang Y, Feng K, Yuan L, Liu Y, Zhang M, Guo K, et al. Compound Danshen Dripping Pill inhibits hypercholesterolemia/atherosclerosis-induced heart failure in ApoE and LDLR dual deficient mice *via* multiple mechanisms. *Acta Pharm Sin B* 2023;**13**:1036−52.

48. Li X, Fan S, Cai C, Gao Y, Wang X, Zhang Y, et al. YAP regulates the liver size during the fasting-refeeding transition in mice. *Acta Pharm Sin B* 2023;**13**:1588−99.

49. Zhu Y, Lei L, Wang X, Chen L, Li W, Li J, et al. The E3 ubiquitin ligase NEDD4-1 protects against acetaminophen-induced liver injury by targeting VDAC1 for degradation. *Acta Pharm Sin B* 2023;**13**:1616−30.

50. Che Z, Song Y, Xu C, Li W, Dong Z, Wang C, et al. Melatonin alleviates alcoholic liver disease *via* EGFR−BRG1−TERT axis regulation. *Acta Pharm Sin B* 2023;**13**:100−12.

51. Wang F, Li Z, Chen L, Yang T, Liang B, Zhang Z, et al. Inhibition of ASCT2 induces hepatic stellate cell senescence with modified proinflammatory secretome through an IL-1α/NF-κB feedback pathway to inhibit liver fibrosis. *Acta Pharm Sin B* 2022;**12**:3618−38.

52. Zhang KK, Chen LJ, Li JH, Liu JL, Wang LB, Xu LL, et al. Methamphetamine disturbs gut homeostasis and reshapes serum metabolome, inducing neurotoxicity and abnormal behaviors in mice. *Front Microbiol* 2022;**13**:755189.

53. Tunc-Ozcan E, Peng CY, Zhu Y, Dunlop SR, Contractor A, Kessler JA. Activating newborn neurons suppresses depression and anxiety-like behaviors. *Nat Commun* 2019;**10**:3768.

54. Ryu JK, Kim SJ, Rah SH, Kang JI, Jung HE, Lee D, et al. Reconstruction of LPS transfer cascade reveals structural determinants within LBP, CD14, and TLR4-MD2 for efficient LPS recognition and transfer. *Immunity* 2017;**46**:38−50.

55. Strati F, Cavalieri D, Albanese D, De Felice C, Donati C, Hayek J, et al. New evidences on the altered gut microbiota in autism spectrum disorders. *Microbiome* 2017;**5**:24.

56. Shi N, Li N, Duan X, Niu H. Interaction between the gut microbiome and mucosal immune system. *Mil Med Res* 2017;**4**:14.

57. Dominguez-Bello MG, Godoy-Vitorino F, Knight R, Blaser MJ. Role of the microbiome in human development. *Gut* 2019;**68**:1108−14.

58. He C, Peng C, Xu X, Li N, Ouyang Y, Zhu Y, et al. Probiotics mitigate *Helicobacter pylori*-induced gastric inflammation and premalignant lesions in INS-GAS mice with the modulation of gastrointestinal microbiota. *Helicobacter* 2022;**27**:e12898.

59. Min Y, Kim MJ, Lee S, Chun E, Lee KY. Inhibition of TRAF6 ubiquitin-ligase activity by PRDX1 leads to inhibition of NFκB activation and autophagy activation. *Autophagy* 2018;**14**:1347−58.

60. Takiishi T, Fenero C, Câmara N. Intestinal barrier and gut microbiota: shaping our immune responses throughout life. *Tissue Barriers* 2017;**5**:e1373208.

61. Thangaraju M, Cresci GA, Liu K, Ananth S, Gnanaprakasam JP, Browning DD, et al. GPR109A is a G-protein-coupled receptor for the bacterial fermentation product butyrate and functions as a tumor suppressor in colon. *Cancer Res* 2009;**69**:2826−32.

62. de Vos WM, Tilg H, Van Hul M, Cani PD. Gut microbiome and health: mechanistic insights. *Gut* 2022;**71**:1020−32.

63. Barberio B, Zamani M, Black CJ, Savarino EV, Ford AC. Prevalence of symptoms of anxiety and depression in patients with inflammatory bowel disease: a systematic review and meta-analysis. *Lancet Gastroenterol Hepatol* 2021;**6**:359−70.

64. Xie J, Liu L, Guo H, Bao Q, Hu P, Li H, et al. Orally administered melanin from *Sepia pharaonis* ink ameliorates depression-anxiety-like behaviors in DSS-induced colitis by mediating inflammation pathway and regulating apoptosis. *Int Immunopharm* 2022;**106**:108625.

65. Xia B, Liu X, Li X, Wang Y, Wang D, Kou R, et al. Sesamol ameliorates dextran sulfate sodium-induced depression-like and anxiety-like behaviors in colitis mice: the potential involvement of the gut−brain axis. *Food Funct* 2022;**13**:2865−83.

66. Dong X, Lu K, Lin P, Che H, Li H, Song L, et al. *Saccharina japonica* ethanol extract ameliorates depression/anxiety-like behavior by inhibiting inflammation, oxidative stress, and apoptosis in dextran sodium sulfate induced ulcerative colitis mice. *Front Nutr* 2021;**8**:784532.

67. Jang HM, Kim JK, Joo MK, Shin YJ, Lee CK, Kim HJ, et al. Transplantation of fecal microbiota from patients with inflammatory bowel disease and depression alters immune response and behavior in recipient mice. *Sci Rep* 2021;**11**:20406.

68. Mirzaei R, Bouzari B, Hosseini-Fard SR, Mazaheri M, Ahmadyousefi Y, Abdi M, et al. Role of microbiota-derived short-chain fatty acids in nervous system disorders. *Biomed Pharmacother* 2021;**139**:111661.

69. Wu H, Xie S, Miao J, Li Y, Wang Z, Wang M, et al. *Lactobacillus reuteri* maintains intestinal epithelial regeneration and repairs damaged intestinal mucosa. *Gut Microb* 2020;**11**:997−1014.

70. Lee YS, Kim TY, Kim Y, Lee SH, Kim S, Kang SW, et al. Microbiota-derived lactate accelerates intestinal stem-cell-mediated epithelial development. *Cell Host Microbe* 2018;**24**:833−46.

71. Sun L, Ma L, Zhang H, Cao Y, Wang C, Hou N, et al. Fto deficiency reduces anxiety- and depression-like behaviors in mice *via* alterations in gut microbiota. *Theranostics* 2019;**9**:721−33.

72. Soto M, Herzog C, Pacheco JA, Fujisaka S, Bullock K, Clish CB, et al. Gut microbiota modulate neurobehavior through changes in brain insulin sensitivity and metabolism. *Mol Psychiatr* 2018;**23**:2287−301.

73. Bercik P, Denou E, Collins J, Jackson W, Lu J, Jury J, et al. The intestinal microbiota affect central levels of brain-derived neurotropic factor and behavior in mice. *Gastroenterology* 2011;**141**:599−609. 601−609.

74. Li JH, Liu JL, Li XW, Liu Y, Yang JZ, Chen LJ, et al. Gut microbiota from sigma-1 receptor knockout mice induces depression-like behaviors and modulates the cAMP/CREB/BDNF signaling pathway. *Front Microbiol* 2023;**14**:1143648.

75. Smith PM, Howitt MR, Panikov N, Michaud M, Gallini CA, Bohlooly YM, et al. The microbial metabolites, short-chain fatty acids, regulate colonic Treg cell homeostasis. *Science* 2013;**341**:569−73.

76. Erny D, Hrabě DAA, Jaitin D, Wieghofer P, Staszewski O, David E, et al. Host microbiota constantly control maturation and function of microglia in the CNS. *Nat Neurosci* 2015;**18**:965−77.

77. Tang CF, Wang CY, Wang JH, Wang QN, Li SJ, Wang HO, et al. Short-chain fatty acids ameliorate depressive-like behaviors of high Fructose-Fed mice by rescuing hippocampal neurogenesis decline and blood−brain barrier damage. *Nutrients* 2022;**14**:1882.

78. Xiao W, Su J, Gao X, Yang H, Weng R, Ni W, et al. The microbiota−gut−brain axis participates in chronic cerebral hypoperfusion by disrupting the metabolism of short-chain fatty acids. *Microbiome* 2022;**10**:62.

79. Wu JT, Sun CL, Lai TT, Liou CW, Lin YY, Xue JY, et al. Oral short-chain fatty acids administration regulates innate anxiety in adult microbiome-depleted mice. *Neuropharmacology* 2022;**214**:109140.